# A Self-Organizing Neural Model of Motor Equivalent Reaching and Tool Use by a Multijoint Arm

**Daniel Bullock, Stephen Grossberg, and Frank H. Guenther**
Boston University

## Abstract

■ This paper describes a self-organizing neural model for eye-hand coordination. Called the DIRECT model, it embodies a solution of the classical motor equivalence problem. Motor equivalence computations allow humans and other animals to flexibly employ an arm with more degrees of freedom than the space in which it moves to carry out spatially defined tasks under conditions that may require novel joint configurations. During a motor babbling phase, the model endogenously generates movement commands that activate the correlated visual, spatial, and motor information that are used to learn its internal coordinate transformations. After learning occurs, the model is capable of controlling reaching movements of the arm to prescribed spatial targets using many different combinations of joints. When allowed visual feedback, the model can automatically perform, without additional learning, reaches with tools of variable lengths, with clamped joints, with distortions of visual input by a prism, and with unexpected perturbations. These compensatory computations occur within a single accurate reaching movement. No corrective movements are needed. Blind reaches using internal feedback have also been simulated. The model achieves its competence by transforming visual information about target position and end effector position in 3-D space into a body-centered spatial representation of the direction in 3-D space that the end effector must move to contact the target. The spatial direction vector is adaptively transformed into a motor direction vector, which represents the joint rotations that move the end effector in the desired spatial direction from the present arm configuration. Properties of the model are compared with psychophysical data on human reaching movements, neurophysiological data on the tuning curves of neurons in the monkey motor cortex, and alternative models of movement control. ■

## 1. THE PROBLEM OF MOTOR EQUIVALENCE

This article introduces a self-organizing neural network model that explains many aspects of the flexibility and robust performance that are characteristic of human reaching behaviors. Central to the model is an analysis of how visual, spatial, and motor representations are formed and combined for the control of goal-oriented reaching.

Spatially defined goals, or targets, can typically be reached using multiple motor means. These multiple motor means derive from having an effector system of higher dimensionality than the goal specification, e.g., a seven degree of freedom (DOF) arm moving a finger along a desired path in three-dimensional (3-D) space. This phenomenon, termed motor equivalence, poses the following problem. How does an organism rapidly and correctly choose among the alternative means that are available to perform spatially defined tasks on different occasions? The model is capable of autonomously learning to combine visual, spatial, and motor information in a way that supports motor equivalent reaching behaviors. In particular, it can learn an inverse kinematic transformation from directions in 3-D space to joint rotations that are capable of moving the arm in these spatial directions. Before describing the model, we discuss key conceptual and experimental considerations that motivate our approach.

### 1.1. The Need for Internal Spatial Representations

Several different phenomena fall under the general heading of motor equivalence. For example, when reaching a target with the tip of the finger, different spatial paths of the finger from initial to final position may be equally effective. Alternatively, goal realization may require a prescribed spatial path, yet allow variability in the effectors used to trace this path, e.g., shoulder and elbow vs. shoulder and wrist. For example, psychophysical studies of reaching, handwriting and drawing have shown that the spatial trajectory is more invariant than the joint rotations, or than force–time patterns (Morasso, 1981, 1986; Teulings, Thomassen, & van Galen, 1986). Production of a prescribed speech sound may also be accomplished using different combinations of articulators (Abbs & Gracco, 1984; Kelso, Tuller, Vatikiotis-Bateson, & Fowler, 1984).

The need for spatial representation in the control of motor-equivalent behaviors is not merely a matter of defining target movements with respect to an external 3-D space. It concerns, more profoundly, the manner in which internal representations of 3-D space develop and can be used to control motor equivalent actions. These internal representations are expressed in both head-centered coordinates and body-centered coordinates since the eyes move within the head, whereas the head, arms, and legs move with respect to the body. The spatial nature of these internal representations is illustrated by the following competence. Imagine that your right hand is moved by an external force to a new position in the dark. Thus, neither visual cues nor self-controlled outflow movement commands are available to encode the right hand's new position. Despite the absence of vision and self-controlled volition, it is easy to move your left hand to touch your right hand in its new location. The motor coordinates that represent the position of your right hand are different from the motor coordinates that your left arm realizes in order to touch it. Some representation needs to exist that mediates between the different motor coordinates of the two arms. This mediating scheme is the internal spatial representation.

The above examples illustrate that different motor plans, whether for the control of one arm or two, are often used to reach a prescribed position in space, and that properly defined internal spatial representations are a prerequisite to discovering a biologically relevant solution of the motor equivalence problem.

As shown below, an internal body-centered representation of 3-D space can be used to help select among the multiple motor means that can realize arm trajectories defined with respect to external 3-D space. A control cycle

$$\mathit{space}_{\mathrm{ext}} \rightarrow \mathit{vision} \rightarrow \mathit{space}_{\mathrm{int}} \rightarrow \mathit{motor} \rightarrow \mathit{space}_{\mathrm{ext}}$$

of self-organized mappings between external 3-D space ($\mathit{space}_{\mathrm{ext}}$) and internal 3-D ($\mathit{space}_{\mathrm{int}}$), mediated by visual and motor representations, carries out this transformation. The model hereby contributes to an analysis of how the "where" or "how" dorsal cortical stream through the posterior parietal region (Anderson, Essick, & Siegel, 1985; Desimone & Ungerleider, 1989; Goodale & Milner, 1992; Ungerleider & Mishkin, 1982; Wise & Desimone, 1988) may utilize combinations of visual, spatial, and motor transformations to control goal-oriented arm movements with motor equivalent properties. As such, the model explicates how a patient such as DF, who suffers from a profound visual-form agnosia that prevents her from indicating her visual orientations either verbally or manually, can nevertheless exhibit normally oriented reaching behaviors (Goodale & Milner, 1992).

We show below how the model can, after an exploratory learning phase, perform accurate reaches with previously inexperienced tools of variable length, clamping of joints, or distortions of visual input by a prism. Blind reaches have also been simulated. The compensatory computations occur automatically within a single reaching movement. The model does not need to learn new commands for each altered movement situation, or to correct an incorrect first movement with subsequent corrective movements. These results clarify how mammalian movement systems can flexibly modify their movement trajectories to achieve desired spatial goals in response to rapidly changing environmental conditions or new environmental demands. Of particular interest is that the ability to accurately position tools—which is a defining characteristic of human societies—may be an automatic consequence of a general motor-equivalent movement competence. These results have previously been briefly summarized in Bullock, Grossberg, and Guenther (1992).

### 1.2. Strategies for Achieving Motor Equivalence

As indicated above, a model of motor equivalent arm movements needs to specify the coordinate frames in which trajectory formation takes place and the nature of the transformation from visual to spatial to motor coordinates. Here we use the terms 3-D *head-centered space* and 3-D *body-centered space* to mean internal representations of the spatial location of a target with respect to the head and body, respectively. *Joint space* is an *n*-dimensional representation wherein *n* is the number of distinct musculoskeletal DOFs. For the purposes of this article, the term *motor coordinates* can be used interchangeably to describe joint space coordinates. Three main types of coordinate transformations may be imagined for relating representations of 3-D body-centered space to joint space for purposes of motor-equivalent reaching:

1. *Motor Trajectory Formation*: The desired target endpoint in 3-D body-centered space is mapped directly to a muscle length or joint angle endpoint. Trajectory formation moves the current arm position continuously toward the desired final arm position in motor (e.g., muscle length or joint angle) coordinates.

2. *Spatial Trajectory Formation with Target Position Mapping* (STP): Trajectory formation is computed in spatial coordinates, and generates a continuous sequence of outflow commands that represent desired end-effector *positions* in 3-D space. A mapping from each spatial position to motor coordinates activates the joint configurations that achieve these positions.

3. *Spatial Trajectory Formation with Direction Mapping* (STD): Trajectory formation again occurs in spatial coordinates, but it generates a continuous sequence of outflow commands that represent desired end-effector

*directions* in 3-D space. A mapping from spatial to motor coordinates transforms each spatial direction into an appropriate change in joint angles that causes movement in the commanded spatial direction.

Motor trajectory formation does not allow direct control of the spatial characteristics of movements. Although such a strategy may be sufficient for totally unconstrained reaches to a target, it cannot be used for spatially defined tasks, such as tracing a figure 8 in a plane. Such a task does not allow the subject to arbitrarily define a path in space between current hand position and target position, because this path is defined by the figure 8 itself. A subject could produce a figure 8 by first defining intermediate target points along the figure 8, then using motor trajectory formation to move between these endpoints. However, accurate tracing would require many intermediate points to be mapped from spatial positions to end effector configurations, thereby transforming the strategy of motor trajectory formation into the strategy of spatial trajectory formation with target position mapping (STP). More generally, many skilled tasks require control of an arm's trajectory in space, not its trajectory in motor coordinates, because objects that the subject wishes to reach, avoid, trace, etc. exist in 3-D space.

Psychophysical studies of human reaching support the idea that trajectory formation occurs in spatial coordinates. In a study of planned arm movements constrained to a horizontal plane, Morasso (1981) noted that while the shape of the tangential hand trajectory velocity profiles remained relatively constant for the different movements, the shapes of the angular velocity profiles for the elbow and shoulder varied (see also Flash & Hogan, 1985; Flash, 1989). The combination of spatial coordinate invariance and motor coordinate variability led him to conclude that the plan was specified in spatial coordinates.

Consideration of motor equivalent capabilities provides a rationale for deciding between the STP and STD control strategies. To exhibit motor equivalence while reaching a spatial target, the effector system needs to possess excess or redundant DOFs. The problem of computing the effector changes needed to realize a spatially characterized goal is called the inverse kinematics problem. The existence of redundant DOF simplies that the inverse kinematics problem is ill-posed and has no unique solution. The fact of motor equivalence thus implies that a one-to-many map must be controlled, whether between 3-D spatial positions and joint configurations in STP or between 3-D spatial directions and joint angle changes in STD.

The main advantage of a one-to-many STD map is as follows. Any linear combination of solutions from spatial directions to joint angle changes generates a trajectory that is continuous in joint space and correctly directed in 3-D space. Joint space continuity obtains because all solutions have the form of joint angle increments with respect to a present fixed configuration $\theta^*$. To see that the direction of the continuation is also correct, suppose that 3-D spatial velocity $\dot{x}$ is related to a joint space velocity vector $\dot{\theta}$ by the approximation

$$\dot{x} = J(\theta)\dot{\theta} \qquad (1)$$

where $J(\theta)$ is the Jacobian of the manipulator. Near the fixed configuration $\theta^*$, system (1) is approximated by the linear system in which $J(\theta^*)$ replaces $J(\theta)$. If for desired $\dot{x}$ and known $\theta^*$ the one-to-many STD mapping computes many solutions $\dot{\theta}^{(i)}$, then the superposition property of linear systems implies that any linear combination of the $\dot{\theta}^{(i)}$ is also a solution, hence is a joint rotation command capable of generating the desired spatial vector $\dot{x}$.

In contrast, the one-to-many map used in the STP strategy is such that solutions do not combine into accurately directed continuations in joint space. Here, the functional relation between a 3-D spatial position vector $x$ and its joint angle configuration $\theta$ is

$$x = f(\theta) \qquad (2)$$

where $f$ is nonlinear. If a desired position $x$ corresponds to many solutions $\theta^{(i)}$, a linear combination of these solutions will usually not itself be a solution, because $f$ is nonlinear. Moreover, most solutions $\theta^{(i)}$ will specify joint configurations that are not adjacent to the current joint configuration $\theta^*$. A process must therefore be implemented to suppress all solutions other than one that is continuous with the current joint configuration $\theta^*$.

In summary, the superposition property of STD systems leads to a simple control strategy for implementing motor equivalence. This strategy can intuitively be described in terms of a *synergy* or synchronous collection of increments to one or more joint angles. Suppose that the motor system associates each of a finite number of synergies to the spatial movement that results when these synergies are activated at a given joint configuration. Then a given movement direction can be achieved by activating in parallel any linear combination of the synergies that produces that movement direction. Continuity of trajectories is assured because the mapping takes the form of small increments to joint angles. Motor equivalence arises when different linear combinations are used on different movement trials.

This property is consistent with data showing that joint angle contributions to a desired spatial motion vary as a function of movement scale and desired accuracy. For example, data from Lacquaniti, Ferrigno, Pedotti, Soechting, and Terzuolo (1987) show that the contribution to a handwriting movement by the elbow and shoulder scales roughly with the size of the figure drawn. If the spatial movements defining the figure are specified as movement directions in 3-D body-centered space, then contributions by the elbow and shoulder can be added to contributions by more distal joints in a linear combination that preserves the movement's spatial form. When movements must be small, the longer limb segments, for which even small joint angle changes produce relatively large end effector displacements, are added to the combination with a very small, possibly zero, coefficient.

### 1.3. Tool Use

Another human motor trait with important implications for trajectory formation models is the ability to perform reaches using tools, such as pointing rods, as the end effector. For example, subjects in Lacquaniti, Soechting, and Terzuolo (1982) performed reaches to targets with lightweight rods strapped to their forearms extending 40 cm beyond the wrist. Even with no practice trials, the trajectories formed by the subjects were very similar to trajectories formed without the rods.

Reaching with tools is difficult to explain in STP systems. Since such reaches can be performed without prior experience with a rod of variable length, the possibility that subjects have learned additional mappings from spatial target positions to joint configurations that compensate for tool length can be discounted. Subjects might still use the STP strategy if they could determine an offset to the spatial target position that compensates for the tool. Instead of moving the tool to the desired target position, the controller would move the hand to a "virtual" target position, formed by adding an appropriate offset to the target position for the tool. This offset depends on the distance and orientation of the tool tip vis-à-vis the hand at the end of the movement. Thus the information required to compute the offset is not directly available at the time when it would be needed, and spatial trajectory formation would be error-prone. In particular, consider what would happen if the calculation of the hand's target position is inaccurate and leaves the tool tip displaced from the target. The most natural correction technique would be to increment joint angles to move the tool tip in the desired direction. This is not possible in a STP system, which does not map spatial directions to joint angle increments. Instead, the STP system must recalculate a new spatial target position for the hand by adding the difference between the tool tip and the target to the hand's target position. Though not impossible, such computations are cumbersome and indirect relative to computations performed in a STD system. In any case, STP systems control at best a two-step movement in which the second movement corrects the error of the first movement.

Tool use is much simpler if spatial movement directions are mapped to changes in muscle lengths or joint angles, as in an STD system. This is so because joint angle changes that move the fingertip in a given direction will move a pointer that is held in the hand in the same direction. Thus, using the difference between the spatial positions of the pointer and the target to specify desired movement directions produces the correct joint angle changes required to move the pointer toward the target. This property is simulated in Section 3.4. Since the system incrementally moves the tool tip closer to the target until the target is reached, there is no need to invoke a separate "correction mode" when the original attempt to reach the target is not fully successful.

### 1.4. Unexpected Perturbations

Another advantage of STD systems is the robustness they exhibit when unexpected events occur in the environment. For example, loss of motion at a particular joint during a reaching movement will cause the actual movement produced by the system to mismatch the desired movement. The effect of such a lost DOF will typically be a movement in the general direction of the target but not in a direct path to the target. If the actual movement direction differs by less than 90° from the desired movement direction, which is typically the case with a single clamped joint in the human arm, an STD system will accurately finish the reach, provided that the geometry of the arm with the clamped joint allows a joint configuration that ends at the target position. This is so because the desired direction of movement continuously reflects the effects of errant movement as long as accurate information about target position and end effector position is available, and the redundant direction mapping always moves the end effector closer to the target, although not necessarily in the optimal direction. This property is simulated in Section 3.5. Moreover, if only unaffected synergies are instated, in particular synergies that do not project to the clamped joint, then the collective activity of these synergies will move the end effector to the target with very little deviation from the desired trajectory.

An STD system is also capable of coping on line with abrupt translations or rotations of the visual field. For example, prism goggles cause target and end effector positions to be misperceived. This can result in an inaccurate estimate of desired movement direction. However, as long as the desired movement direction as perceived by the observer differs by less than 90° from the actual direction of the target with respect to the end effector, direction mapping under continuous visual guidance moves the end effector closer to the target, as shown in the simulation in Section 3.7. Continuous updating of the desired movement direction takes into account the errant movement, so deviations do not accumulate.

To complete our comparison of STP and STD systems, we note one disadvantage of STD systems, albeit a disadvantage that is also characteristic of human performance. Bock and Eckmiller (1986) have shown that when humans make a series of movements to visible targets in the absence of visual feedback of hand position, then there is an accumulation of hand positioning errors over the series. Such accumulation is expected in an STD system, but would not occur in an STP system. In agreement with the assumptions of our model, which implements an STD system, Bock and Eckmiller (1986) concluded that "the pointing performance as observed in the present study is better compatible with the alternative hypothesis that amplitudes, i.e. distances between objects, are coded in the sensory space, and are transformed into movement amplitudes in the motor space" (p. 457).

Consideration of the movement problems described in this section thus suggests the existence of a mapping from spatial directions to joint rotations, hereafter called a *direction-to-rotation transformation*. The following sections present a self-organizing neural network that learns such a transformation, thus explaining how the properties described in the previous paragraphs may arise in neural systems. This network is called a DIRECT model to emphasize both the key role of *direction* mapping and the fact that direction mapping leads to goal-oriented trajectories that move *directly* to the target under a wide variety of movement conditions. The acronym DIRECT stands for DIrection-to-Rotation Effector Control Transform.

## 2. OVERVIEW OF THE DIRECT MODEL

Figure 1 illustrates the major functional components that enable a DIRECT model to implement a coordinate transformation from spatial directions to joint rotations. The right-hand column of this figure shows a cascade of processing stages that allow external target position to guide changes in the end effector position during a reaching task. First, the spatial coordinates of the target must be computed. In the DIRECT model, a 3-D body-centered representation of target position is computed by a neural network that combines visual, eye position, and head position information. Neural networks that perform the transformation using retinal, oculomotor, and neck-motor signals are described in Greve, Grossberg, Guenther, and Bullock (1992), Grossberg, Guenther, Bullock, and Greve (1992), and Guenther, Bullock, Greve, and Grossberg (1992). Second, a spatial difference vector (DV) is computed by comparing the target position representation with a representation of end effector position, measured in the same body-centered coordinate frame. The spatial DV codes both direction and magnitude information. It specifies the spatial displacement needed to bring the end effector into contact with the target. Third, a spatial-to-motor transformation computes the joint angle changes, or rotations, that move the end effector along the spatial DV toward the target. Because this transformation computes joint rotations that produce desired spatial motion directions, it can alternatively be called a direction-to-rotation transformation. Computation of appropriate joint angle changes requires information about both the direction of the spatial DV and the current joint configuration. Thus, another input to the direction-to-rotation stage, coming from a stage coding joint angles, is depicted. Finally, the fourth major stage in the feedforward cascade integrates the angle increments or decrements commanded by the direction-to-rotation signals. The outputs from this stage specify angular settings for all joints and thus control end effector position. Ensuring a close relationship between these commanded joint angle changes and actual effector position changes requires a solution to the inverse dynamics problem. Our discussion proceeds on the assumption that this problem is solved by additional neural circuits, such as the spinal cord and cerebellar circuits analyzed in the FLETE model of Bullock and Grossberg (1989, 1991; also see Bullock & Contreras-Vidal, 1992; Bullock, Contreras-Vidal, & Grossberg, 1992).

Three distinct feedback loops appear in Figure 1. The first uses the joint angle integrator to update the direction-to-rotation transform. The joint angle integrator also updates a multimodal stage that can use either joint configuration inputs or visually derived inputs to compute the spatial coordinates of the end effector. This requires an intermediate motor-to-spatial transformation to convert joint configuration information into the spatial coordinate frame used for trajectory formation. This spatial representation of end effector position is compared to the spatial representation of target position to compute the spatial DV, thereby closing the second feedback loop. Proprioceptive information can also be used in these capacities, forming additional feedback loops (not shown) to augment the two loops just discussed.

The third and longest feedback loop is an external loop that exists whenever the end effector is visible. Then its spatial coordinates can be computed by transforming its retinal images into a 3-D body-centered spatial representation. This is fed to the multimodal stage where it can be combined with joint configuration inputs to estimate end effector position.

In summary, during the movement cycle, any discrepancy between target position and end effector position is registered at the spatial DV stage, whose outputs are transformed into appropriate joint rotations. As the joints rotate, internal feedback ensures that the direction-to-rotation transform is adjusted to reflect the new joint configuration. As the movement proceeds, either internal or external feedback to the multimodal stage updates the internal representation of end effector position. Because this representation changes in the direction of the target, the spatial DV is driven toward zero. The movement self-terminates when the internal spatial representations of end effector position and target position coincide and the spatial DV equals zero.

As noted above, both internal and external feedback loops exist for updating the internal representation of end effector position. The internal loops are faster and can be used to avoid lag-based instability. Updating via the internal feedback loop is therefore preferable during

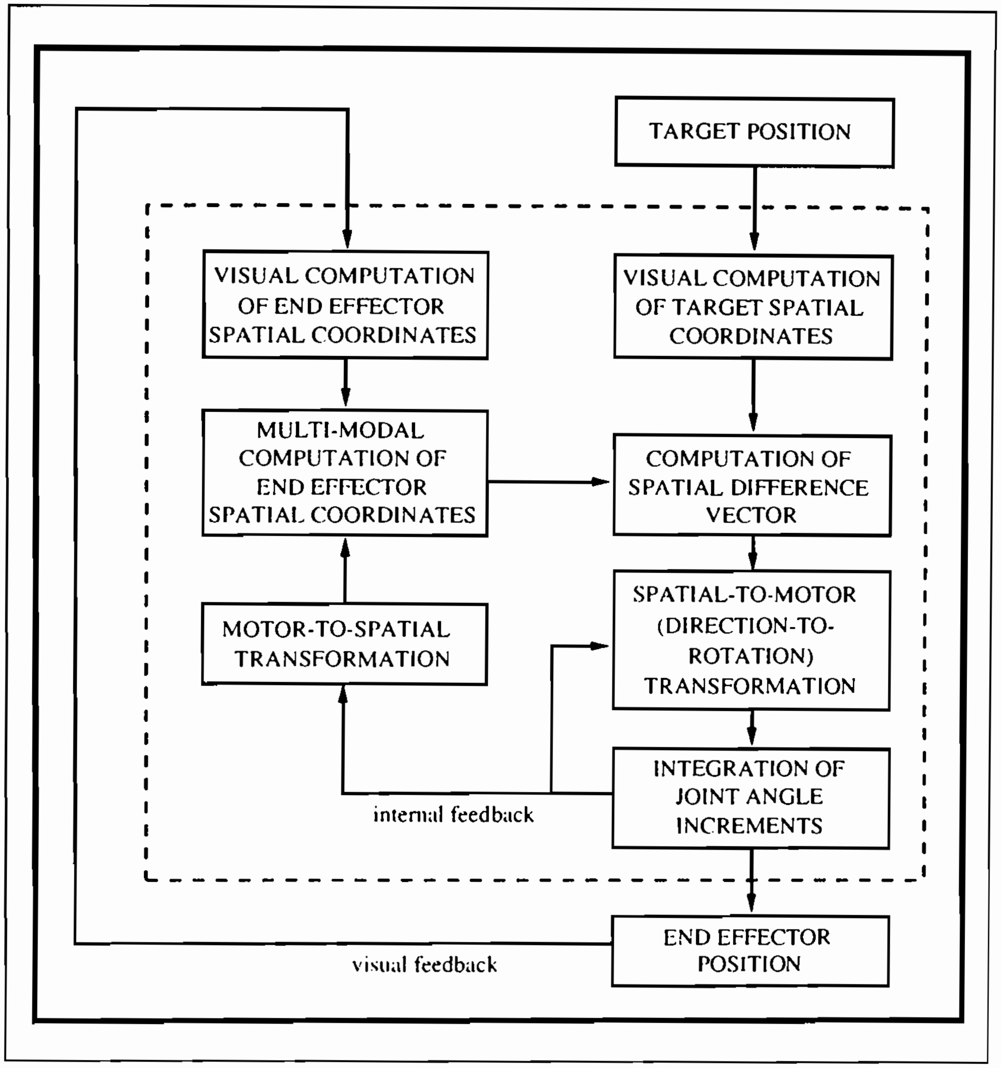
TARGET POSITION
VISUAL COMPUTATION OF END EFFECTOR SPATIAL COORDINATES
VISUAL COMPUTATION OF TARGET SPATIAL COORDINATES
MULTI-MODAL COMPUTATION OF END EFFECTOR SPATIAL COORDINATES
COMPUTATION OF SPATIAL DIFFERENCE VECTOR
SPATIAL-TO-MOTOR (DIRECTION-TO-ROTATION) TRANSFORMATION
MOTOR-TO-SPATIAL TRANSFORMATION
INTEGRATION OF JOINT ANGLE INCREMENTS
internal feedback
END EFFECTOR POSITION
visual feedback

**Figure 1.** Processing stages of the DIRECT model.

very rapid movements or higher velocity segments of slower movements. For purposes of accuracy, however, the slower visual feedback is preferable. These considerations suggest two devices for optimizing performance. First, it may be useful to make the visual feedback dominant when movement rate is low and internal feedback dominant when movement rate is high. Second, it maybe useful to distribute speed over the course of movement so as to allow a terminal low-speed phase for accurate visually guided homing.

## 2.1. Relationship to the VITE Model of Trajectory Formation

The existence of a low-speed homing phase in spatially accurate point-to-point movements is well established (Woodworth, 1899; Howarth & Beggs, 1972; Nagasaki, 1989). This and several other kinematic properties of point-to-point motions, notably synchronous contraction of synergetic muscles and voluntary control of movement speed, have received a unified explanation in terms of the Vector Integration to Endpoint, or VITE, model of Bullock and Grossberg (1988a, 1988b), which is schematized in Figure 2a. The VITE model introduced several of the main computational processes out of which the DIRECT model is fashioned, including continuous computation of a difference vector (DV) from the difference between a target position vector (TPV) specifying the intended movement goal, and an outflow movement command called the present position vector (PPV). The DV, in turn, is multiplied by a speed-controlling GO signal before being integrated at the PPV stage to form the outflow movement command. The original VITE model dealt only with trajectory formation in joint space. The Adaptive VITE, or AVITE, model of Gaudiano and Grossberg (1991) extended VITE to learn coordinate transformations within the motor trajectory generator. The AVITE model was further generalized in Gaudiano and Grossberg (1991) to the Vector Associative Map, or VAM, model to show how coordinate transformations from spatial positions to joint configurations could also be learned using DV stages repeated in a hierarchical

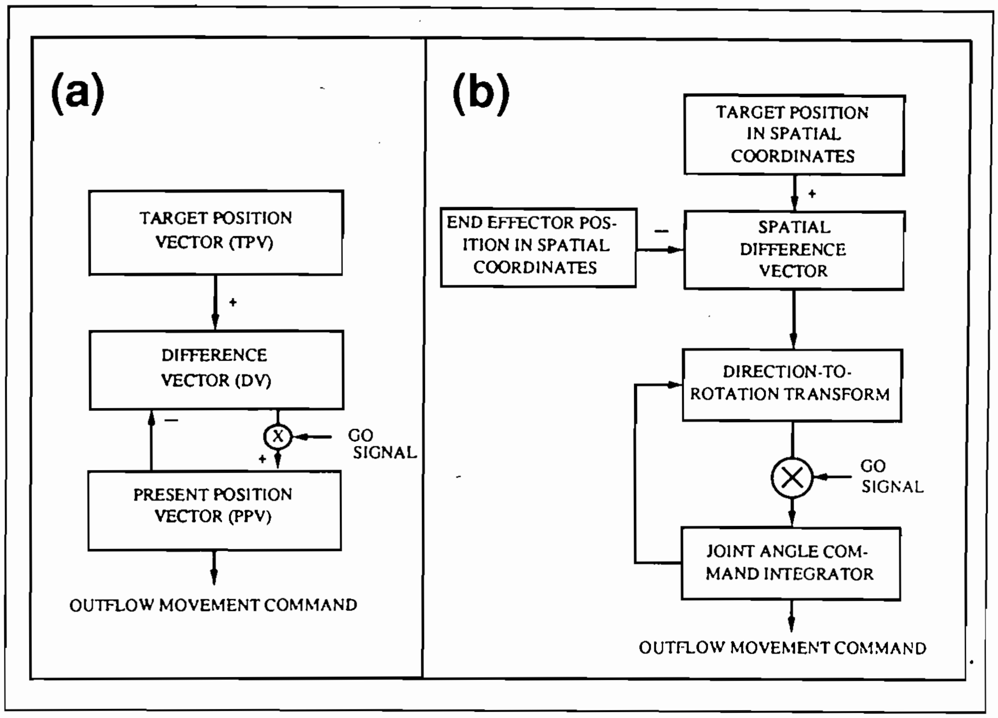
(a)
TARGET POSITION VECTOR (TPV)
+
DIFFERENCE VECTOR (DV)
−
X
GO SIGNAL
+
PRESENT POSITION VECTOR (PPV)
OUTFLOW MOVEMENT COMMAND
(b)
TARGET POSITION IN SPATIAL COORDINATES
+
END EFFECTOR POSITION IN SPATIAL COORDINATES
−
SPATIAL DIFFERENCE VECTOR
DIRECTION-TO-ROTATION TRANSFORM
GO SIGNAL
JOINT ANGLE COMMAND INTEGRATOR
OUTFLOW MOVEMENT COMMAND

**Figure 2.** (**a**) Block diagram of the VITE model of trajectory formation. (**b**) DIRECT implementation allowing voluntary control of movement duration and generation of realistic velocity profiles as in VITE.

cascade of spatial-to-motor processing stages. Analysis of this model and the limitations of STP models set the stage for developing the present STD model by focusing on the key role of spatial and motor DVs in the control of movement.

The DIRECT model thus remains broadly consistent with those aspects of the VITE and VAM designs that allow both voluntary control of movement duration and generation of realistic velocity profiles. In particular, both properties appear in the DIRECT model if a movement-gating GO signal multiplies the joint rotation commands prior to their integration at the joint angle command stage, as in Figure 2b. If the GO signal is zero, a spatial DV and desired rotations are computed, but no movement occurs. When the GO signal becomes positive, end effector movement rate is proportional to its magnitude multiplied by the magnitude of the spatial DV. The decline of the spatial DV magnitude during movement leads to movement slowing even if, as is usually assumed, the GO signal grows during movement.

The next few sections define the DIRECT model in more precise computational terms and illustrate how it works. Section 2.2 describes the two main types of neural representations used in the DIRECT model: *map* and *vector* representations. Section 2.3 describes learning of the motor-to-spatial and direction-to-rotation mappings. Section 3 presents the results of several simulations designed to illustrate motor equivalence, tool use, robustness under unexpected perturbations, and blind reaching. Section 4 provides a detailed description of the current DIRECT implementation, including the equations used in computer simulations. Section 5 summarizes neurophysiological studies of motor cortical cell properties and relates these data to the current implementation as well as possible alternative implementations of the mapping from spatial directions to joint angle increments. Section 6 compares the DIRECT model with alternative models of movement control.

## 2.2. Classifying Processing Stages into Maps and Vectors

The DIRECT model uses a number of processing stages that can profitably be classified into *maps* and *vectors*. Map codes are *position* codes and vector codes are *feature* codes. Thus, in a map, different locations in a spatial array of neurons represent the data to be coded. This spatial array typically approximates a 2-D surface, or a laminar organization of cell populations that is parameterized by a 2-D surface (Hubel & Wiesel, 1977; Mountcastle, 1957). In a vector code, each neuron or population of neurons represents a different feature, or combination of features. The activity levels of these neurons are the coordinates of the vector code. Changes in the relative and absolute amounts of featural activation across all the vector coordinates constitutes the code.

Figure 3 shows a simple example that illustrates map and vector neural representations. Consider the problem of representing the point $p$ in the 2-D space shown in Figure 3a. In Figure 3b, a *position map* (PM) is used to represent $p$. In this representation, a large number of neuron populations, or nodes (shown as black circles), are used to represent the 2-D space. Each neuron population, or node, codes a small region of the 2-D space, such that the node's firing rate or activity level (shown as the bar above the circle) is maximal when the quantity

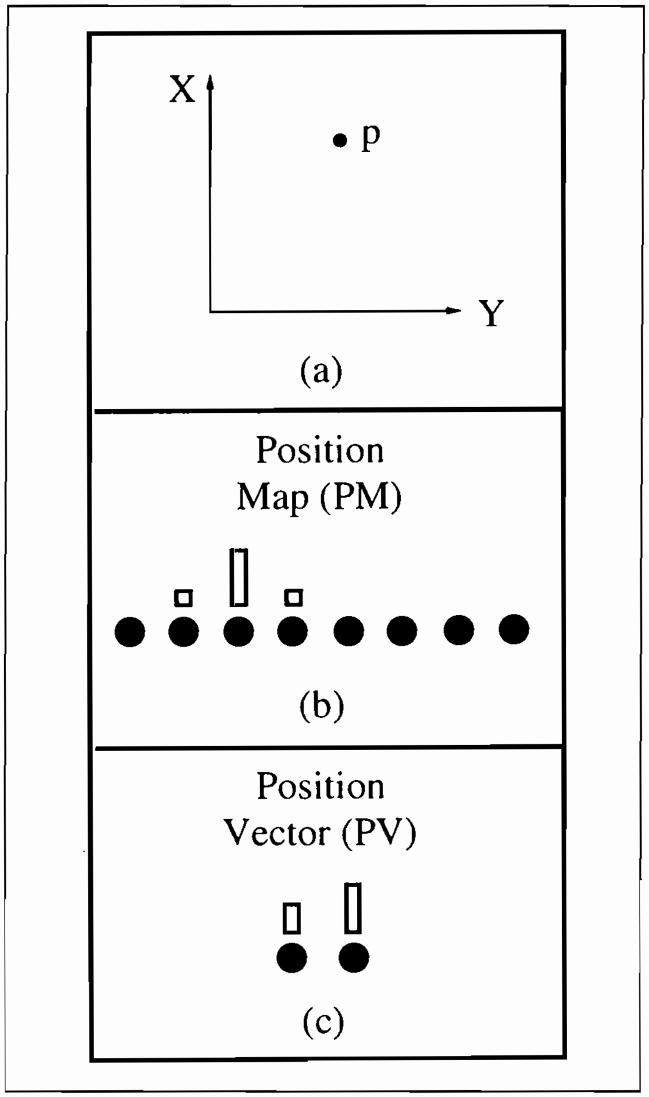

**Figure 3.** (**a**) An example of 2-D space. (**b**) A position map representing the point *p* in this space. (**c**) A position vector representing the point *p*.

being represented is within this small region. Thus, a single population in the map of Figure 3b is maximally active, and this population codes a small region of the input space, including the point *p*. In Figure 3c, a *position vector* (PV) is used to represent the point *p*. In this representation, one neuron's firing rate increases for increased position along the *x* axis, and a second neuron's firing rate increases for increased position along the *y* axis. Thus, the pattern of activity across the two neurons represents the point *p* in the 2-D space.

In addition to representing absolute positions, vectors and maps can be used to represent the difference (i.e., distance and direction) between two positions. A *difference* or *direction map* (DM) can be used to represent the length and direction of a commanded movement in a map whose maximally activated node changes with these parameters. A *difference* or *direction vector* (DV) represents the same movement properties by changes in the balance of feature activations. For example, a DV is formed in the VITE model by subtracting a present position vector (PPV) from a target position vector (TPV). This DV codes the distance and direction from the present position to the target position using featural activations computed in joint coordinates. In the DIRECT model, the term *direction vector* is used rather than the term *difference vector* to emphasize the directional, as opposed to positional, nature of the quantities being represented.

Grossberg (1989) articulated the distinction between maps and vectors by noting that both a difference map (DM) and a difference vector (DV) appear to be used for purposes of eye movement control. In the deeper layers of monkey superior colliculus, a difference map (DM) code exists wherein each map location tends to code a different combination of movement length and direction (Mays & Sparks, 1980, 1981; Sparks, 1978, 1991; Sparks & Jay, 1987; Sparks & Mays, 1981). The most eccentric locations tend to code the longest movements. Changing the 2-D polar angle of locations in the map tends to change movement direction. Exciting cells at a prescribed map location tends to cause a saccadic eye movement of corresponding length and direction. In the monkey motor cortex, a DV code exists wherein each cell tends to generate a broad unimodal tuning curve of direction preference that may include 180 degrees of movement directions (Evarts & Tanji, 1974; Georgopoulos, 1986, 1989; Georgopoulos, Kalaska, Caminiti, & Massey, 1982; Georgopoulos, Kalaska, Crutcher, Caminiti, & Massey, 1984; Georgopoulos, Schwartz, & Kettner, 1986; Tanji & Evarts, 1976). Movement amplitude tends to covary with the firing rate of cells in their direction of maximum sensitivity (Fu, Suarez, & Ebner, 1992).

The concepts and notation of maps (M) and vectors (V) enables a systematic vocabulary to be developed for the processing stages that are described below for the control of motor equivalent reaching. This notation also suggests a systematic shorthand for conceptualizing the multiplexed combinations of constraints to which cells at the various processing stages are tuned. For example, we will encounter below a PDM stage to encode in a topographic map (M) the direction (D) in which the limb is commanded to move when it is in a particular present position (P). Another distinction concerns whether a representation encodes external spatial locations with respect to the body, or internal joint angles of a limb. The subscripts "s" and "m," for "spatial" and "motor," are used to denote this distinction. Thus the notation $PPM_m$ signifies a processing stage at which the joint angles (m) of the present limb position (PP) are represented by a topographic map (M). Notation $DV_s$ signifies a processing stage at which movement directions (D) in external 3-D space (s) are represented by a feature vector (V). Notation $PDM_{ms}$ signifies a processing stage at which information about the joint angles of the present limb position

($P_m$) is combined with information about desired movement directions in external space ($D_s$) in a topographic map ($M$). The notation $PDM_{ms} \rightarrow DV_m$ thus means that when the limb attains a particular present joint position ($P_m$) and a desired spatial direction of movement ($D_s$) is selected, then this conjoint constraint ($PDM_{ms}$) is used to activate $DV_m$, and thus the limb joints are rotated by the proper relative amounts to realize the desired movement direction in space. The transformation $PDM_{ms} \rightarrow DV_m$ is sometimes called the direction-to-rotation transform in the subsequent discussion.

## 2.3. Autonomous Learning of the DIRECT Transformations during Motor Babbling

Figure 4 illustrates the DIRECT model that was used in our computer simulations of motor equivalent reaching. This figure fills in several processing stages left out of Figure 1. Figure 4 shows that the DIRECT model contains two learned transformations, which are indicated by filled semicircles. A spatial-to-motor, or direction-to-rotation, transformation in the right processing stream commands the motor actions needed to carry out a spatially defined trajectory. A motor-to-spatial transformation in the left processing stream allows motor information regarding end effector position to be used in place of visual information when performing reaches without visual feedback. Learning in the DIRECT model is achieved through autonomously generated repetition of an action-perception cycle, which generates the associative information needed to learn these transforms. Such a cycle was called a *circular reaction* by Piaget (1963). A circular reaction endogenously creates movements in babies during a *motor babbling* phase, and leads to learning of transformations among representations that are correlated through these movements. After learning takes place, the movements may later be carried out in an intentional, or goal-oriented, manner.

Motor babbling is energized by an endogenous random generator, or ERG, whose activations are integrated to generate movement commands (Gaudiano & Grossberg, 1991). In the DIRECT model, ERG activations excite the $DV_m$ stage, which encodes motor commands for rotating the joints. The output of the $DV_m$ stage is integrated at the $PPV_m$ stage, whose outputs control joint angles and, therefore, the end effector location. In this way, ERG activity causes spontaneous arm movements during the motor babbling stage. The network uses the information generated by these spontaneous arm movements in several ways. Visual feedback provides information about the positions and directions of movements in 3-D space. Internal feedback provides information about the joint configurations that generate these movements. The network is designed to combine these multiple sources of information in a manner that solves the motor equivalence problem. The present discussion refines the description of processing stages given in Section 5 by using a consistent map-vector notation and including the stages that are needed to learn the spatial-to-motor and motor-to-spatial transformations.

Visual feedback accomplishes two tasks during motor babbling: it provides information about the *position* of the hand for tuning the motor-to-spatial mapping and it provides information about the *direction* of hand movement for tuning the direction-to-rotation mapping. To accomplish the direction-to-rotation mapping, three types of information need to be properly calibrated and combined: the $DV_s$, which specifies the spatial direction in which the hand must move to contact the target; the $DV_m$, the motor direction in which the joints rotate to generate $DV_s$; and the $PPV_m$, the present position of the end effector. Information from $DV_s$ and $PPV_m$ need to be combined to unambiguously command the proper joint rotation $DV_m$ by which to move in spatial direction $DV_s$ when the joints start in the configuration $PPV_j$m. This combination process occurs at $PDM_{ms}$, which mediates the direction-to-rotation transformation from $DV_s$ to $DV_m$. These calibration and combination processes are suggested to occur as follows.

During motor babbling, the endogenously moving end effector is a salient visual target. As the system visually tracks its own end effector, the present position and target position information about the end effector coincide. Correspondingly, visual information about end effector position is passed to both the $PPV_s$ and $TPV_s$ stages. The $PPV_s$ stage relays its information to the $PPV_{sm}$ stage. Both the $TPV_s$ stage and the $PPV_{sm}$ stages relay signals to the $DV_s$ stage. The $DV_s$ neurons represent the difference between end effector position as derived from the excitatory $TPV_s \rightarrow DV_s$ pathway and a slightly delayed version of end effector position from the inhibitory $PPV_s \rightarrow PPV_{sm} \rightarrow DV_s$ pathway. The slight delay results from the additional synapse in the latter pathway. The result is that $DV_s$ represents the spatial direction of end effector movement.

Information regarding the direction of end effector movement, represented at the $DV_s$ stage during motor babbling, drives learning of the direction-to-rotation transformation. To convert $DV_s$ activations into effective reaching behaviors, each $DV_s$ must be transformed into a $DV_m$, which produces movement in the corresponding spatial direction, that is, spatial directions need to be converted into joint rotations. As noted above, the appropriate $DV_m$ to learn depends on the configuration of the arm when the $DV_s$ is computed. The conjoint activation of the $PDM_{ms}$ stage by both the $PPV_m$ stage and the $DV_s$ stage activates a small number of cells in the $PDM_{ms}$ map. These cells then learn the babbled $DV_m$ activity that is producing the motion direction registered at the $DV_s$ stage.

How do the *vector* stages $PPV_m$ and $DV_s$ get transformed into a *map* stage $PDM_{ms}$ that combines a motor position map ($P_m$) with a spatial direction ($D_s$)? It is assumed that the motor vector stage $PPV_m$ generates

**Figure 4.** Block diagram of a self-organizing DIRECT model in map-vector notation.

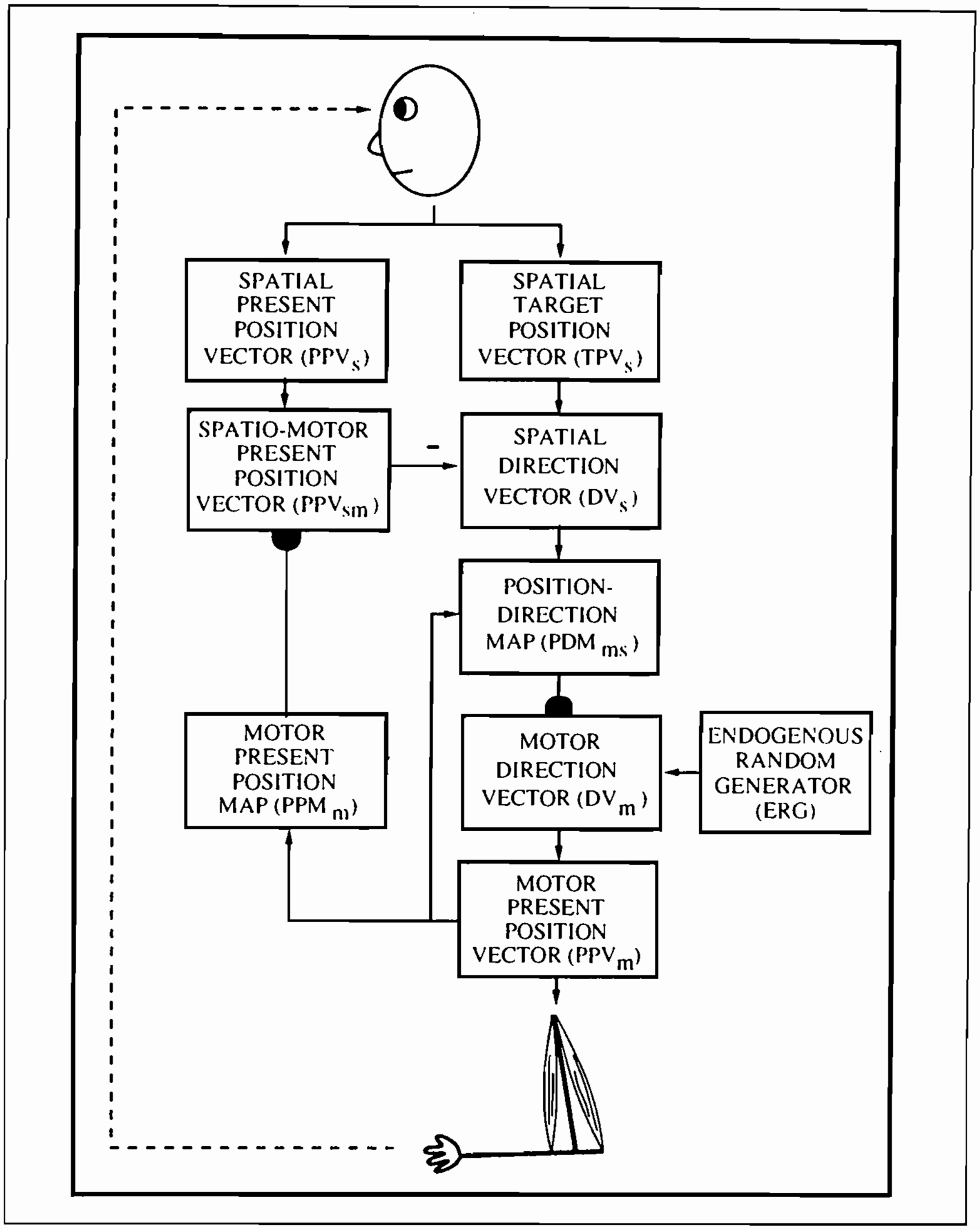
SPATIAL PRESENT POSITION VECTOR (PPV$_S$)
SPATIAL TARGET POSITION VECTOR (TPV$_S$)
SPATIO-MOTOR PRESENT POSITION VECTOR (PPV$_{Sm}$)
-
SPATIAL DIRECTION VECTOR (DV$_S$)
POSITION-DIRECTION MAP (PDM$_{mS}$)
MOTOR PRESENT POSITION MAP (PPM$_m$)
MOTOR DIRECTION VECTOR (DV$_m$)
ENDOGENOUS RANDOM GENERATOR (ERG)
MOTOR PRESENT POSITION VECTOR (PPV$_m$)

corollary discharges as well as outflow movement commands. These corollary discharges may be combined directly with the vector $DV_s$ to form $PDM_{ms}$ via a self-organizing feature map (Grossberg, 1976, 1982; Grossberg & Kuperstein, 1986, 1989; Kohonen, 1988; Malsburg, 1973; Willshaw & Malsburg, 1976). Alternatively, the vector representation $PPV_m$ may first be converted via a self-organizing feature map into $PPM_m$, after which $PPM_m$ is combined with the spatial direction vector $DV_s$ to form $PDM_{ms}$.

A motor-to-spatial transformation is also learned during motor babbling. The goal of this transformation is to convert a motor representation $PPV_m$ of the present end effector position into a visual representation $PPV_s$ of present end effector position. This transformation is suggested to occur via the learned transformation, described above, from $PPV_m$ to $PPM_m$, followed by a learned association from $PPM_m$ to $PPV_{sm}$. In this way, a joint configuration coded at the $PPV_m$ stage learns to predict the corresponding spatial position of the end effector as represented through vision at $PPV_s$.

In summary, during motor babbling, the *ERG* spontaneously generates motor vectors $DV_m$, which are integrated into arm movements by the $PPV_m$ stage. The arm movements draw visual attention to the end effector. As a result, spatial $DV_s$ vectors are computed which, conjointly with $PPV_m$ feedback signals, enable the $PDM_{ms}$ map to learn an appropriate $DV_m$ with which to move in the corresponding spatial direction $DV_m$ when the end effector is at $PPV_m$. Simultaneously, joint configurations coded by the $PPM_m$ stage are associated through learning at the $PPV_{sm}$ stage with the corresponding spatial positions $PPV_s$ of the end effector as perceived through vision.

These movements and learning events during motor babbling are not goal-oriented. The babbled movements are endogenously activated and the learning events correlate spatial and motor representations that are coactivated by the babbled movements. During subsequent goal-oriented reaching movements, the target is not typically the end effector, so the information coded at $TPV_s$ and at $PPV_s$ is not the same. The DIRECT model is designed such that after motor babbling ends, when a target other than the end effector activates $TPV_s$, the difference between present position of the end effector at $PPV_{sm}$ and the target position at $TPV_s$ is computed at $DV_s$, and the arm is steered toward the target by activating an appropriate series of $DV_m$ vectors to move the arm in the desired direction. If visual feedback of the end effector is not available during the reach, then the motor pathway $PPV_m \rightarrow PPM_m \rightarrow PPV_{sm}$ is used to estimate end effector position rather than the visual pathway $PPV_s \rightarrow PPV_{sm}$. In particular, after learning, the DIRECT model uses gating signals to direct the flow of visual information to the $PPV_s$ block if the visually attended spatial position corresponds to the end effector, or to the $TPV_s$ block if the visually attended spatial position corresponds to a goal-oriented movement target. This requires the developing system to incorporate some mechanism for differentiating between self-generated movements of the hand and other potential targets of visual attention (moving or stationary) in the visual field. A possible mechanism for providing this "self" vs. "other" distinction is outlined in Figure 5. Another developmentally important constraint incorporated in the model is that visual information about end effector position takes precedence over motor corollary discharges, when both types of information are available at the $PPV_{sm}$ stage.

Before characterizing the DIRECT model processing stages computationally, we summarize computer simulations that illustrate the types of motor equivalent movements that the DIRECT model is capable of controlling after it learns its circular reaction.

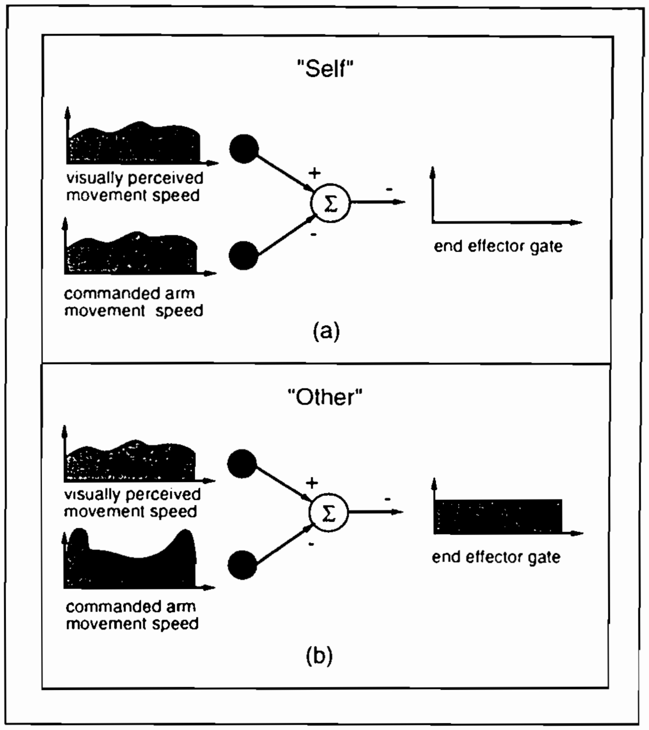
"Self"
visually perceived movement speed
commanded arm movement speed
+
-
Σ
-
end effector gate
(a)
"Other"
visually perceived movement speed
commanded arm movement speed
+
-
Σ
-
end effector gate
(b)

**Figure 5.** Possible gating mechanisms for distinguishing self-generated arm movements from other visually perceived movements. This model gating mechanism directs visual signals to $TPV_s$ or $PPV_s$. It enables an infant network to distinguish visual input corresponding to its arm ("self") from visual input corresponding to other targets ("other"). If not, visual information corresponding to targets other than the arm would erode the map learning that occurs when the visual input does correspond to the arm. One way to distinguish between "self" and "other" is to compare movement speed in the visual pathway with internal arm movement velocity commands. A match between the temporal patterns of these speeds, as in (**a**), indicates with high probability that the object being visually attended to is the infant network's arm. The comparator output can then be used as an inhibitory end effector gating signal; that is, a zero value of this signal allows visual information to flow to the $PPV_{sm}$ block, and a nonzero value blocks this flow, thereby preventing erosion of the learned motor-to-spatial map in Figure 4.

## 3. COMPUTER SIMULATIONS OF REACHING BEHAVIORS

The simulations use a three joint arm in two dimensions. The origin of the spherical coordinate frame used in the simulations lies in the same plane as the shoulder (corresponding to a 2-D subject whose shoulder and egocenter lie in the same plane). Thus, for reasons clarified in Section 4.1, spherical coordinates $R$, $\phi$, and $\theta$, with $\theta = 0$, are used to represent target and end effector positions. The wrist is treated simply as an extra degree of freedom with properties similar to those of the elbow and shoulder. The claim is not made that wrist movements are equivalent to elbow and shoulder movements. Rather, the wrist is included here to provide redundancy; it forces the model to coordinate three DOFs to move the end effector in a 2-D plane. Appendix A provides the kinematic equations for the simulated arm model. A fourth-order Runge–Kutta method was used for integration with a time step of 0.4. Each training trial consisted of 50 time steps.

### 3.1. Training

The model's feedforward and feedback mappings were trained by instating randomly chosen initial joint configurations, then generating random $DV_m$ activities and using visual feedback to register end effector position and movement direction. Training was always done with visual feedback and without tools, clamped joints, or visual shifts. The steps in training were

1. Initialize all weights to 0.
2. For the first trial and every tenth subsequent trial, randomly generate a new initial arm configuration.
3. For each trial (a) endogenously generate a $DV_m$ and move the arm based on this command. This corresponds to infant "motor babbling"; (b) update activities of all stages based on the equations given in Section 4 on Formal Specification of the DIRECT Model; and (c) adjust $PDM_{ms} \rightarrow DV_m$ adaptive weights and $PPM_m \rightarrow PPV_{sm}$ adaptive weights according to Eqs. (14) and (21), respectively, below.
4. If more trials remain, go back to Step 2.

Typical training sessions included generation of 40,000 $DV_m$s, which consumed approximately 18 min of CPU time on a Silicon Graphics Iris 4D/240GTX.

### 3.2. Performance

After training, the DIRECT model is capable of reaching to arbitrary positions in the workspace. To do this, a target position is first loaded into the $TPV_s$ block in the model as illustrated by the boldface lines in Figure 6a. As the focus of visual attention, the target position is neurally represented within a coordinate frame that approximates the 3-D spherical coordinates ($R$, $\phi$, $\theta$) with $\theta = 0$. As in Figure 5, a volitional gating signal indicating that a movement target is being attended directs this visual information to the $TPV_s$ block, where it remains stored throughout the reach. Figure 6b and 6c shows the flow of information for reaches with and without visual guidance, respectively. In Figure 6b, the visual representation of end effector position is gated to the $PPV_s$ block. When available, visual information dominates over proprioceptive or corollary discharge information concerning end effector spatial position at the $PPV_{sm}$ block. The visual representation of end effector position is compared to the stored target position at the $DV_s$ block in Figure 6b; $DV_s$ thus represents the desired movement direction. The pathway $DV_s \rightarrow PDM_{ms} \rightarrow DV_m$ performs the learned direction-to-rotation transformation, and integration of the $DV_m$ activities at the $PPV_m$ stage produces movement of the arm in the desired direction. Current position of the end effector is constantly updated at the $PPV_{sm}$ stage so that $DV_s$ always represents the direction from the end effector to the target. In Figure 6c, visual information of end effector position is unavailable, so end effector spatial position at $PPV_{sm}$ is estimated using the learned motor-to-spatial transformation of pathway $PPV_m \rightarrow PPM_m \rightarrow PPV_{sm}$. This estimate is compared to the stored target position at the $DV_s$ stage, and movement in the desired direction is carried out as in the visually guided case.

### 3.3. Simulation I—Normal Reaching

In simulation I, the model performs visually guided reaches to the target positions with no clamped joints or tool extensions. The results of this simulation provide a baseline for comparison to later simulations, which show more challenging properties of the model. The trajectories of the end effector produced by the model depend on the feedforward $PDM_{ms} \rightarrow DV_m$ mapping. These trajectories closely match the trajectories in Figure 7b that were produced by linear interpolation in the spherical coordinate frame. One of these simulated trajectories is shown in Figure 8a. Thus the surface structure of the motor behavior gives little hint of the internal coordinate transformation. The Figure 8a trajectories of the end effector, wrist, and elbow roughly approximate those of

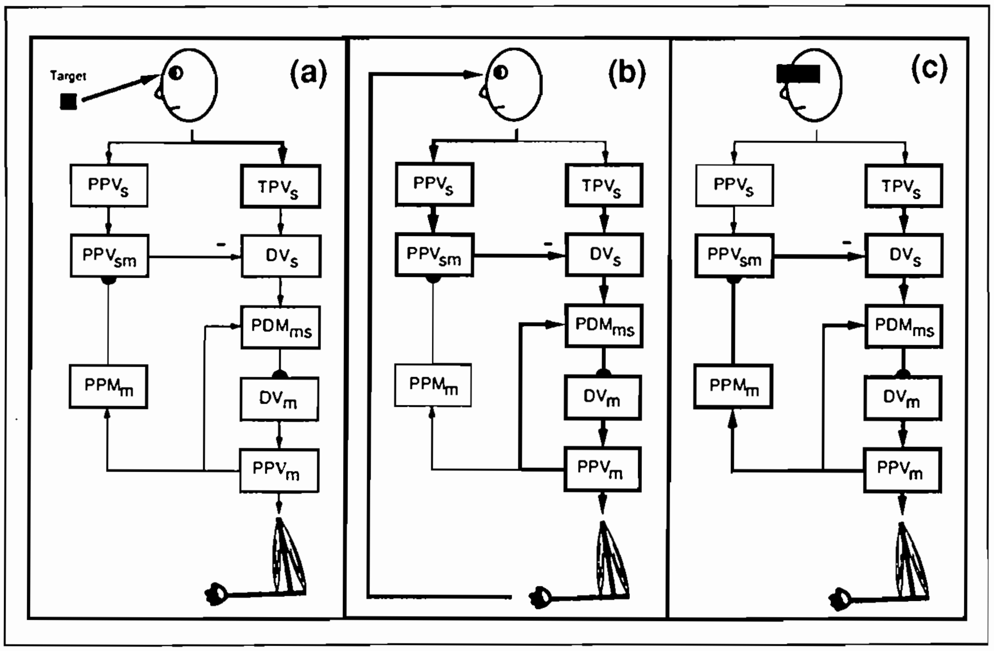

**Figure 6.** (**a**) Loading a visually perceived movement target. (**b**) Flow of information for performing a visually guided reach. (**c**) Flow of information for performing a blind reach.

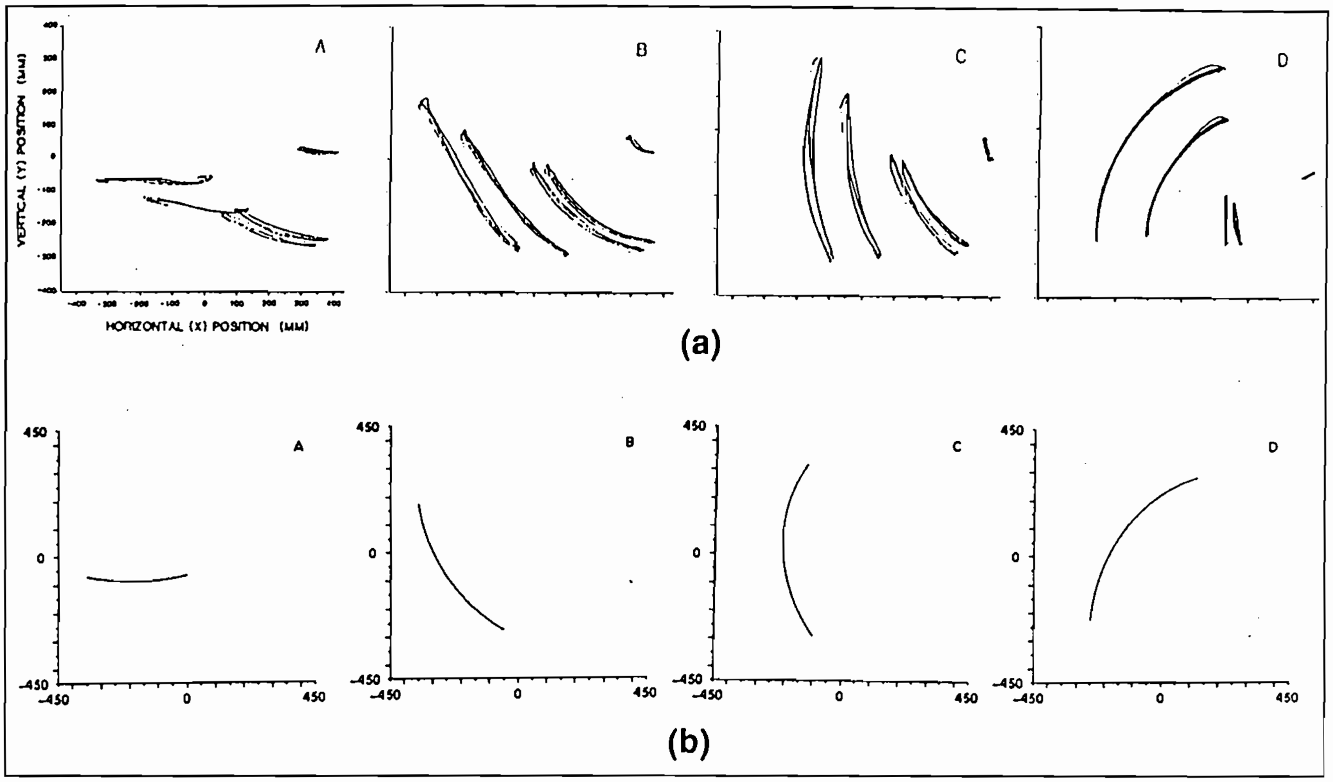

**Figure 7.** (**a**) Trajectories from Hollerbach et al. (1986). Units are millimeters, with the shoulder located near (0,0). Trajectories are shown for shoulder, elbow (shown as two trajectories), wrist, and fingertip. (**b**) Simulation of the Hollerbach et al. (1986) fingertip trajectories using linear interpolation in spherical coordinate space.

human subjects in the Hollerbach, Moore, and Atkeson (1986) experiments, as in panel C of Figure 7a. See Section 4.1 for further discussion of these data.

### 3.4. Simulation II—Reaching with a Tool

For simulation II, a tool was added to the hand of the model during performance trials, but there was no retraining with the tool. Reaches were performed under visual guidance, with the visual data for end effector position computed from the tool end rather than the hand. The tool used in the simulation was 150 mm long and was attached to the hand at an angle of 160°. Similar results were achieved with tools of many lengths attached at many different angles with respect to the hand. One simulated reach and the relative length of the tool are shown in Figure 8b. Compare the trajectories formed with the tool in Figure 8b to the reaches without a tool in Figure 8a.

### 3.5. Simulation III—Clamped Joint

For this simulation, the elbow joint of the model was clamped at an angle of 140° during performance trials, but there was no retraining with the clamped joint. As shown in Figure 8c, the model successfully performs reaches to targets despite this joint blockage. To achieve the effect of clamping the joint at a single angle, the $PPV_m$ activity components corresponding to the elbow angle command were fixed throughout the movement. Thus the internal feedback of joint angle remained accurate throughout the movement, and correct $PDM_{ms}$ cells continued to be activated as the movement evolved. The same net result could be achieved with external clamping even if $PPV_m$ cells associated with elbow angle control continued to integrate their inputs, provided that proprioceptive feedback from the clamped joint could correct the internal command feedback prior to the $PDM_{ms}$ stage. Bullock and Grossberg (1988a) have described how arm inflow signals can correct $PPV_m$ commands under conditions where external forces prevent the arm from obeying outflow movement commands.

### 3.6. Simulation IV—Blind Reaching

Simulation IV was run to test the learned feedback mapping from limb configuration to spatial position of the end effector; that is, the mapping that allows corollary discharge information from the $PPV_m$ stage to replace visual information about limb spatial position in defining desired direction of movement. Turning off visual input to the $PPV_{sm}$ stage forced use of corollary discharge

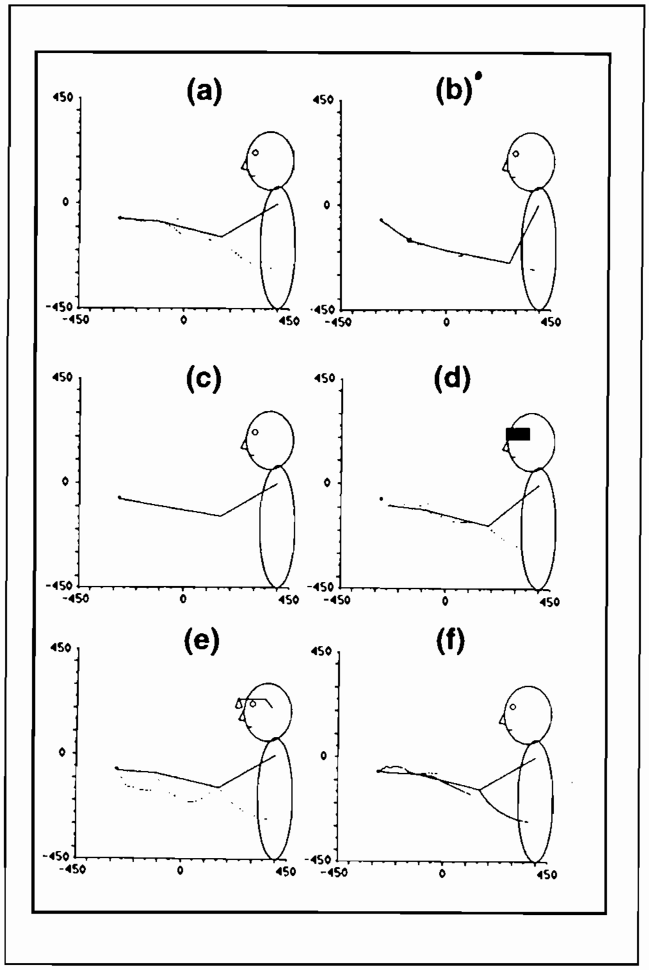

**Figure 8.** Trajectories formed by the model for one of the target positions of Hollerbach, Moore, and Atkeson (1986; see panel C of Figure 7a). The small square represents the target position that the model is attempting to reach. (**a**) Trajectory formed by the model during an unconstrained reach. (**b**) Trajectory formed by the model using a pointer for reaching. (**c**) Trajectory formed by the model with the elbow clamped at 140°. (**d**) Trajectory formed by the model using corollary discharge information of end effector position in place of visual information (i.e., blind reaching). (**e**) Trajectory formed by the model under continuous inspection of the end effector after a visual shift causes a mismatch between perceived movement direction and actual movement direction. (**f**) Trajectory formed by the model with nonlinear muscle plant activities.

information, which is routed through the $PPM_m$ stage, to update the end effector position.

A resulting trajectory is shown in Figure 8d. The trajectory in this figure is nearly identical to the visually guided reach shown in Figure 8a. This verifies the correctness of the learned internal feedback mapping between limb configuration, as represented by the vector of joint angle settings, and spatial position of the end effector. This mapping is useful for blind reaches and for very fast reaches, which might suffer oscillations if visual information (which *in vivo* is delayed due to slow arm mechanics) were used to update the end effector position estimate used at the $DV_s$ stage. Visually guided reaches are more accurate than blind reaches, as also occurs *in vivo* (e.g., Bock & Eckmiller, 1986; Ott & Eckmiller, 1988; Soechting & Flanders, 1989). In the model, this is due to the coarseness of the coding of joint space by cells in the $PPM_m$ map. That is, each cell in $PPM_m$ codes a small region of joint space, and the projected activity to $PPV_{sm}$ from $PPM_m$ is constant within this joint space region. Because of this, all joint configurations within the small region of joint space that includes the target position will be treated equally, and movement stops as soon as the arm enters this region. A more finely grained $PPM_m$ representation could control correspondingly more accurate blind reaches.

### 3.7. Simulation V—Visual Shift

Simulation V verifies performance under a visual shift, as might be produced by prism goggles. A shift in either horizontal or vertical angle of the target due to prism goggles does not change the movement direction perceived by the subject, since both target position and current end effector position are both shifted by an equal amount in spherical coordinates. However, had spatial directions been specified in some other coordinate frame, such as Cartesian coordinates, a mismatch would occur between perceived and actual movement direction to the target. To simulate this situation, perceived motion direction was directly shifted by 30° from actual motion direction to target in the simulation. That is, the $DV_s$ stage output was rotated by 30° before being sent to the $PDM_{ms}$ stage.

A resulting simulated trajectory is shown in Figure 8e. Under continuous visual guidance, the model successfully completes the trajectories using shifted visual information from the end effector. This outcome depends on the STD map from spatial directions to joint angle rotations and would not be produced by an STP map from target positions to joint angles. An STP system would need a two-or-more-step "correction" mode, as mentioned in Section 1.2. Had only the shifted visual target position $TPV_s$ been stored and the reach performed using motor feedback $PPM_m$ about end effector position, the reach would not have been accurate.

### 3.8. Simulation VI—Nonlinear Rotation Commands

In this simulation, the $PPV_m$ stage integration of the $DV_m$ is replaced in both the training and performance phases with a nonlinear integration process that is described in Section 4.5. The resulting model approximates a system with a nonlinear relationship between joint rotation commands and the actual rotation achieved. Nonlinear muscle properties often require larger command increments to produce a given joint angle increment at more extreme joint angles. Although compensatory cerebellar learning tends to linearize muscle response (Grossberg & Kuperstein, 1986, 1989), the present simulation shows that residual nonlinearities may be compensated by the DIRECT controller. As shown in Figure 8f, the altered model produces trajectories quite similar to those observed in the previous simulations.

Figures 9, 10, and 11 show the DIRECT trajectories that are generated under conditions (I)–(VI) above with targets at different locations in the workspace.

## 4. FORMAL SPECIFICATION OF THE DIRECT MODEL

We now specify the DIRECT model computationally. The first task is to summarize how a 3-D body-centered spatial representation that approximates spherical coordinates is self-organized by the model.

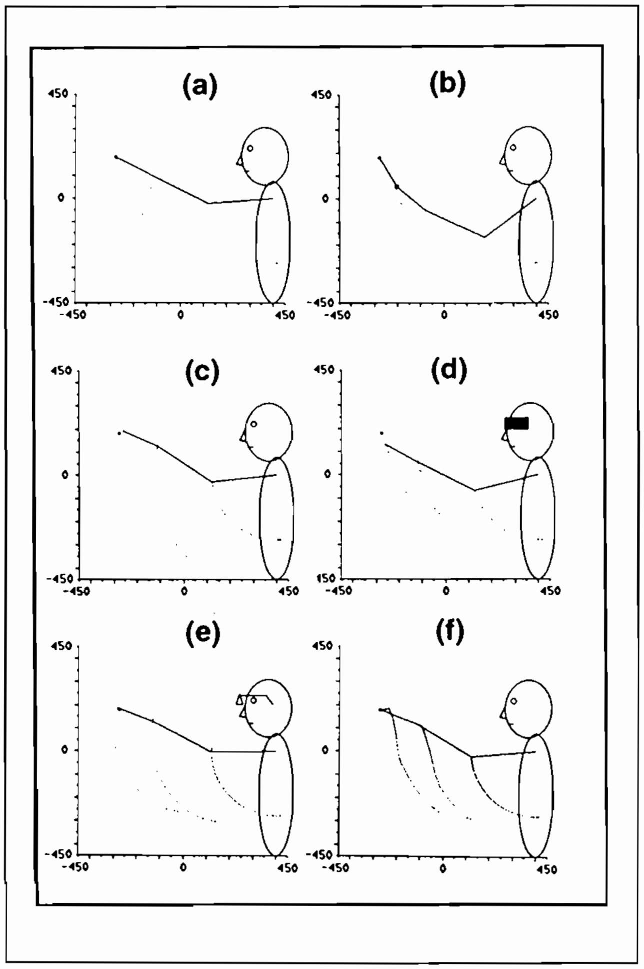

**Figure 9.** Simulated trajectories to a different target location under the conditions of Figure 8.

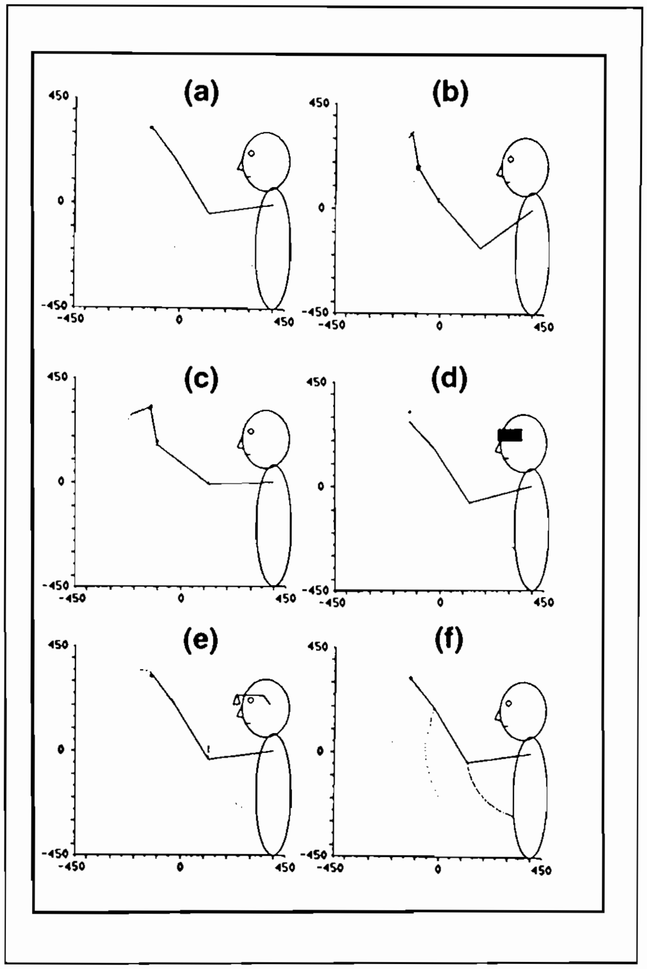

**Figure 10.** Simulated trajectories to a different target location under the conditions of Figure 8.

### 4.1. Self-Organizing a Body-Centered Representation of 3-D Target Position

A self-organizing body-centered representation of 3-D space was modeled in Bullock, Greve, Grossberg, and Guenther (1992), Greve et al. (1992), Grossberg et al. (1992), and Guenther et al. (1992). These articles describe how several kinds of information may be combined to form a body-centered 3-D spatial representation. The retinal positions in both eyes that are excited by a visually perceived target, the positions of both eyes in the head, and the position of the head in the body are combined by the model via a self-organizing learning process to form an internal 3-D spatial representation of target position in body-centered coordinates. The term *target* here denotes the object of visual attention. This is not necessarily the same as the target of a reaching movement. In particular, the end effector is often the target of visual attention in the DIRECT model.

This spatial representation exploits the bilateral symmetry of the body, notably the opponent organization of many muscles into agonist–antagonist pairs. The first part of the model shows how a head-centered representation

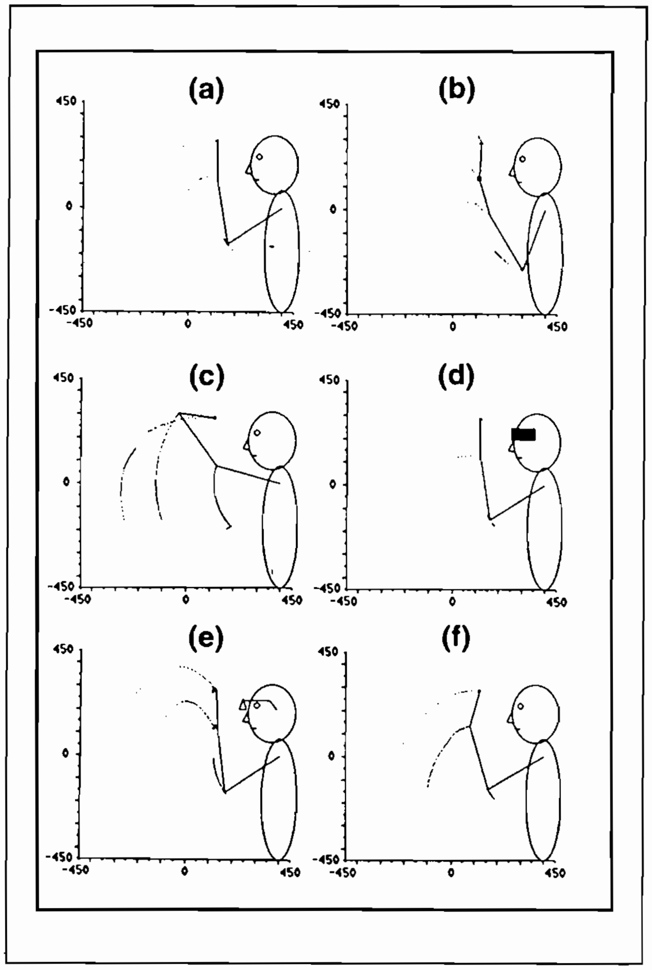

**Figure 11.** Simulated trajectories to a different target location under the conditions of Figure 8.

of 3-D target position is formed when the target is foveated by both eyes (Bullock, Greve, Grossberg, and Guenther, 1992; Greve et al., 1992). This model network combines corollary discharges from the outflow movement commands to the extraocular muscles of both eyes. Two successive opponent processing stages convert these corollary discharges into a head-centered cyclopean representation of the foveated target's 3-D position. The origin of this cyclopean representation lies between the eyes. Its coordinates estimate the horizontal polar angle $\theta$, vertical polar angle $\phi$, and the binocular vergence $\gamma$ of the foveated target with respect to this cyclopean origin in the head. Psychophysical data are discussed to support the biological relevance of this model.

The second part of the model shows how to learn a head-centered representation of 3-D target position, even if a target is initially registered at nonfoveated retinal positions (Grossberg et al., 1992). This representation can be used to generate a movement signal whereby the eyes can saccade to foveate a target, and sets the stage for learning a body-centered representation for reaching toward a target. The head-centered representation combines the opponent motor representation of where the eye is looking, with retinal information concerning the binocular location of the target with respect to the present gaze position. Learning uses a vector associative map, or VAM, which had previously also been used to learn parameters for arm trajectory control as well as a simpler type of head-centered target representation (Gaudiano & Grossberg, 1991). The final part of the model shows how a body-centered representation can be learned by combining the head-centered representation with signals from the neck concerning the position of the head in the body (Guenther et al., 1992). Again VAM learning is used.

All of these representations build upon the cyclopean head-centered representation ($\gamma$, $\phi$, $\theta$). Due to the close relationship between the vergence $\gamma$ and the radial distance $R$ (Greve, et al., 1992), the latter variable is used in the present simulations. Thus, the internal representation is a vector of six neuron (or neuron population) activities, grouped into three agonist–antagonist pairs, that represent the three body-centered spherical coordinates. The origin of the coordinate frame lies directly between the two eyes when the head is pointed straight ahead, and it remains fixed with respect to the torso when the head angles (horizontal or vertical) are changed. The angle $\theta$ represents the horizontal angle of a target with respect to straight ahead of the body, and the angle $\phi$ represents the vertical angle of the target with respect to straight ahead of the body. The coordinate $R$ represents the distance from the origin to the target. Specifically, this internal representation approximates the following equations:

$$v_1 + v_2 = 1 \tag{3}$$

$$\theta = -90^\circ + 180^\circ \times v_2 \tag{4}$$

$$v_3 + v_4 = 1 \tag{5}$$

$$\phi = -90^\circ + 180^\circ \times v_4 \tag{6}$$

$$v_5 + v_6 = 1 \tag{7}$$

$$R = \alpha v_6 + \beta \tag{8}$$

where the $v_i$ are cell activity levels forming the visual representation vector $\mathbf{v}$, and $\alpha$ and $\beta$ provide a linear fit for $R$ in terms of $v_6$ throughout the workspace. For simplicity, the current simulations were done in two dimensions using the above equations for $R$ and $\phi$ only, corresponding to movements in a plane where $\theta$ remains fixed.

An internal representation based on spherical coordinates has several advantages. First, as noted above, this coordinate frame relates closely to the anatomy of the eye muscles. The anatomy of the arm also relates more closely to a spherical coordinate frame than to a Cartesian frame, since arm movements due to shoulder rotation correspond to changes primarily in the spherical angles θ and ϕ, whereas bending of the elbow relates primarily to the spherical coordinate $R$. This property proves useful for transformation from spatial coordinates to arm trajectories.

Figure 7a from Hollerbach et al. (1986) shows measured trajectories for the fingertip, wrist, elbow (shown as two trajectories), and shoulder during free reaches by human subjects in the sagittal plane through the shoulder, with the shoulder located near (0,0). Figure 7b shows simulated trajectories formed between the endpoints of the fingertip paths of Figure 7a using linear interpolation in the body-centered spherical coordinate space of Eqs. (3)–(8). Although interpreted by Hollerbach et al. (1986) as being a result of joint space interpolation, Figure 7b indicates that the Figure 7a trajectories are also consistent with spherical space interpolation, thus providing evidence of similarities between the two coordinate frames. Finally, as shown in Guenther et al. (1992), spherical coordinates allow a transformation to be learned from a head-centered to a body-centered internal representation using corollary discharges from neck position commands. How such a transformation would be achieved in Cartesian frames is not readily apparent. It should be noted, however, that a spherically based coordinate frame is not a necessary condition for satisfactory performance by the DIRECT network. Other vector representations of external space, including Cartesian, could also be used.

### 4.2. Computation of the Spatial Difference Vector

Both target position and end effector position are represented in the body-centered coordinate system specified above in terms of the $v_i$. Henceforth, let $E = (e_1,e_2, \ldots, e_6)$ be the visual representation of end effector position ($PPV_s$ in Fig. 4), $M = (m_1,m_2, \ldots, m_6)$ the multimodal representation of end effector position ($PPV_{sm}$ in Fig. 4), and $T = (t_1,t_2, \ldots, t_6)$ the visual representation of target position ($TPV_s$ in Fig. 4). The spatial difference vector $DV_s$ is denoted by $D = (d_1,d_2, \ldots, d_6)$, where

$$d_i = t_i - m_i \qquad (9)$$

$i = 1, \ldots, 6$. During training, the magnitude of the $DV_s$ is small and represents the movement direction of end effector position, formed by taking the difference between current end effector position and end effector position one time step earlier (corresponding to the additional one synapse delay in the $PPV_s \rightarrow PPV_{sm} \rightarrow DV_s$ pathway as compared to the $TPV_s \rightarrow DV_s$ pathway). During performance of a visually guided reach, the target's position may initially be quite far from the end effector's position. The magnitude of the $DV_s$ can therefore be quite large during performance. However, since cells in the position-direction map ($PDM_{ms}$ in Fig. 4) are sensitive to $DV_s$ movement direction and insensitive to $DV_s$ amplitude, the larger $DV_s$ values encountered during performance are transformed into the appropriate motor vector $DV_m$ that was learned for movement in the desired direction.

### 4.3. The Position-Direction Map

The $PDM_{ms}$ stage of Figure 4 contains a map of cells, each of which is maximally sensitive to a particular spatial direction in a particular position of joint space. The activity level $c_k$ of a cell in this map is 1 if the $DV_s$ codes that cell's preferred spatial direction and the $PPM_m$ codes the same cell's preferred limb configuration. Cell activity falls off to 0 as $DV_s$ and $PPM_m$ signals deviate from preferred.

This kind of selective cellular receptivity can be achieved by adaptive filter networks such as self-organizing feature maps. However, for these simulations it sufficed to create a population of cells with suitable preformed receptive fields. The number of cells was determined by the need to restrict each cell's receptive field to a sufficiently small region of possible spatial directions and joint configurations. Dividing spatial directions into 30 angular zones (each representing 12° of direction in a plane) and the range of each joint into 7 angular zones yielded 30 × 7 × 7 × 7, or 10,290 cells at the $PDM_{ms}$ stage.

More precisely, to simulate the three DOF planar arm reaching to targets in a 2-D space, we let $\mathbf{d} = (d_1,d_2)$ represent the desired motion direction specified by the $DV_s$ stage. Coordinates $d_1$ and $d_2$ correspond to the desired direction components in the two spatial coordinates of the 2-D movement plane. Similarly, let $\mathbf{a} = (a_1,a_2,a_3)$ represent the current joint configuration, with coordinates $a_1$,$a_2$, and $a_3$ defining the three joint angles. Then a cell $k$ responds selectively if its input is

$$I_k = \sum_{i=1}^{2} d_i^k + \sum_{j=1}^{3} a_j^k \qquad (10)$$

where

$$d_i^k = \begin{cases} d_i & \text{if } d_i^{k-} < d_i < d_i^{k+} \\ 0 & \text{otherwise} \end{cases} \qquad (11)$$

and

$$a_j^k = \begin{cases} a_i & \text{if } a_j^{k-} < a_j < a_j^{k+} \\ 0 & \text{otherwise} \end{cases} \qquad (12)$$

The $d_i^{k-}$ and $d_i^{k+}$ denote minimum and maximum values of $d_i$ specific to cell $c_k$, respectively, and $a_j^{k-}$ and $a_j^{k+}$ denote minimum and maximum values of $a_j$ specific to cell $c_k$. The parameters $d_i^{k-}$, $d_i^{k+}$, $a_j^{k-}$, and $a_j^{k+}$ were chosen such that one and only one cell received the maximal input for a given motion direction and joint configuration.

It would be sufficient to allow only that unique cell with the maximal input at any moment to learn the current pattern at the $DV_m$ stage. Fewer training trials are needed if partially activated cells with neighboring receptive fields are also allowed to learn. In addition, learning signals generated by $PDM_{ms}$ cells should not be so large as to drive learning to equilibrium on a single trial. These properties can be achieved if the $PDM_{ms}$ stage contrast enhances and normalizes the activity distribution defined by the $I_k$. Use of a large neighborhood early in training results in quick learning of an approximate mapping from $PDM_{ms}$ cells to $DV_m$ cells, and slow reduction of this neighborhood size as training proceeds increases map accuracy through time. Grossberg (1986, Section 23) has described how neighborhood size may be made to *automatically* shrink during adaptive tuning of a suitably defined self-organizing feature map.

To reduce the length of time needed to simulate the system on a serial computer, the parallel network interactions described above were typically approximated. In particular, $I_k$ was computed only for cells with $d_j^k > 0$ for all $j$. Among those cells, the seven most active were allowed to generate positive learning signals $c_k$ for the first 50% of learning trials. Learning was then further restricted to the three most active cells for the final 50% of learning trials. Moreover, the maximal $c_k$ was always given a value of 1.0, while the maximum of the remaining positive $c_k$ ranged from 0.5 early in learning to 0.2 late in learning. The same qualitative results hold for any similar scheme, and no attempt was made to optimize parameters used in this portion of the simulation.

### 4.4. Learning the Direction-to-Rotation Transform

The neural populations that represent the joint rotation vector $DV_m$ code a set of joint rotation commands to be integrated by populations at the $PPV_m$ stage, as in Figure 4. These $DV_m$ populations receive inputs from two sources: *ERG* cells and $PDM_{ms}$ cells. During training, the ERG activates $DV_m$ cells with random values $x_i$ for a brief period during the action–perception cycle. During performance, the ERG is off, and the signals $c_k z_{ki}$ from the active $PDM_{ms}$ sites $k$ alone activate the $DV_m$ populations. Thus, the $DV_m$ activities $r_i$ may be approximated by the following equation:

$$r_i = x_i + \sum_k c_k z_{ki} \qquad (13)$$

where $x_i$ is the *ERG* activation and $z_{ki}$ is the adaptive weight, or *LTM* trace, from population $k$ in $PDM_{ms}$ to population $i$ in $DV_m$. Equation (13) is an algebraic equation, rather than a differential equation, because $r_i$ is assumed to track its inputs at a fast integration rate.

The $r_i$ activities are organized into antagonistic pairs, with each antagonistic pair corresponding to movements about a single joint. The notation $r_i^E$ and $r_i^I$ will be used to denote excitatory and inhibitory members of an antagonistic pair corresponding to joint angle $\theta_i$, with each member in the pair given a separate subscript in Eq. (13). For example, a nonzero activity $r_1^E$ results in an increase in joint angle $\theta_1$, and a non-zero activity $r_1^I$ results in a decrease in joint angle $\theta_1$; see Eqs. (15) and (16). During each training cycle, *ERG* activation $x_i$ of one $DV_m$ cell of each antagonistic pair is chosen from a uniform distribution between 0 and 1, and *ERG* activation of the other cell in the pair is set to 0 for that training cycle. All $x_i = 0$ when the ERG is off, and the $c_k z_{ki}$ activation is small early in training. Thus $x_i$ dominates $r_i$ during training and $\Sigma_k c_k z_{ki}$ dominates $r_i$ during performance.

The adaptive weights, or LTM traces, $z_{ki}$ between $PDM_{ms}$ cell $k$ and $DV_m$ population $i$ were initialized at zero and modified according to the following learning equation:

$$\frac{dz_{ki}}{dt} = \gamma c_k(-\delta z_{ki} + r_i) \qquad (14)$$

where $\gamma$ is a small learning rate parameter, and $\delta$ is a decay rate parameter. The parameter values $\gamma = 1$ and $\delta = 0.2$ were used in the simulations. Equation (14) is an example of outstar learning (Grossberg, 1968). During outstar learning, activating $c_k$ opens a learning gate which allows the LTM trace $z_{ki}$ to approach, or track, $r_i$ via steepest descent. Outstar learning improves on Hebbian learning by allowing synaptic weights to either increase or decrease during learning. Proofs exist for deterministic convergence to a weight vector proportional to a single postsynaptic vector or centroid of vectors (Grossberg, 1968, 1969, 1982) or for stochastic convergence to the centroid of a set of postsynaptic vectors (Clark & Ravishankar, 1990a, 1990b). An important condition for convergence is that the postsynaptic activities $r_i$ and adaptive weights $z_{ki}$ are bounded. The $r_i$ remain bounded provided that the differential equation whose equilibrium behavior is approximated by Eq. (13) is a membrane, or shunting, equation (Grossberg, 1973, 1976). Then Eq. (14) guarantees that the $z_{ki}$ are bounded within the same range.

### 4.5. Linear and Nonlinear Integration of Joint Rotation Vectors

The $PPV_m$ populations integrate signals from corresponding $DV_m$ populations to produce an outflow command specifying a set of joint angles (Fig. 4). Each $PPV_m$ cell codes the angle of a particular joint and receives input from two $DV_m$ cells: an excitatory input from a $DV_m$ cell coding increments to that joint angle, and an inhibitory input from a $DV_m$ cell coding angle decrements (Bullock & Grossberg, 1988a; Gaudiano & Grossberg, 1991). Thus, the net input integrated by the $PPV_m$ cell is the difference between the activities of the two corresponding $DV_m$ cells. Two versions of this integration process are used in the simulations. The first version integrates the net

*DV*$_m$ value, with equal changes occurring in joint angle for a given net *DV*$_m$ activity regardless of where the joint is in its range of motion, until the joint reaches the end of its range of motion. In the second version, a given net *DV*$_m$ activity causes smaller changes to the *PPV*$_m$ component when the joint nears the extremes of its range. The latter version is used to illustrate the ability of the model to operate correctly with a nonlinear relationship between joint rotation commands and the actual joint angle changes that result. Although formulated as a nonlinear relationship between *DV*$_m$ activities and changes in *PPV*$_m$ activities, this version is functionally equivalent to a system with a nonlinear relationship between *PPV*$_m$ commands and the actual limb configuration.

The updating rule used for the first version (linear integration) is:

$$\frac{d}{dt} a_i = \epsilon(r_i^E - r_i^E) \tag{15}$$

where $\mathbf{a} = (a_1,a_2,a_3)$ is the *PPV*$_m$ vector, $a_i$ is the angle command for joint $i$, $r_i^E$ and $r_i^I$ are the corresponding excitatory and inhibitory *DV*$_m$ cell activities, respectively, and $\epsilon$ is an integration rate parameter. In the simulations, $a_i$ specified the joint angle $\theta_i$ in degrees, and an integration rate parameter $\epsilon = 0.25$ was used. For the second version (nonlinear integration), the updating rule was:

$$\frac{d}{dt} a_i = \epsilon(r_i^E - r_i^I)\left[|\psi_{\max} - \psi_{\text{rest}}| - |\psi_i - \psi_{\text{rest}}|\right] \tag{16}$$

where $\psi_i$ is the angle of the joint corresponding to $a_i$, $\psi_{\max}$ is the maximum angle of this joint, and $\psi_{\text{rest}}$ is assumed to be $(\psi_{\max} - \psi_{\min})/2$.

## 4.6. Mapping from Limb Configuration to Multimodal Representation of End Effector Position

Section 2.3 described the value of having an internal pathway from the *PPV*$_m$ for updating the multimodal spatial coordinate representation *PPV*$_{sm}$ of end effector position. Figure 12 shows a blowup of the stages that were used to learn this feedback mapping. As shown, outputs of the limb configuration vector at *PPV*$_m$ are sent to the *PPM*$_m$ stage where these vectors are classified into different map locations, e.g., via a self-organizing feature map. Because such self-organization was not our focus, we once again sought an efficient approximation sufficient for demonstrating DIRECT properties. To assure sufficient resolution for the blind reaching simulation, we divided the range of each joint into 25 angular zones and created 25 × 25 × 25 cells at the *PPM*$_m$ stage to cover the entire space of configurations possible for the 3-joint limb. Thus the activation function for sites $k$ in *PDM*$_s$ was

$$j_k = \begin{cases} 1 & \text{if } d_j^{k-} < a_j < d_j^{k+}, \text{ for all } a_j \\ 0 & \text{otherwise} \end{cases} \tag{17}$$

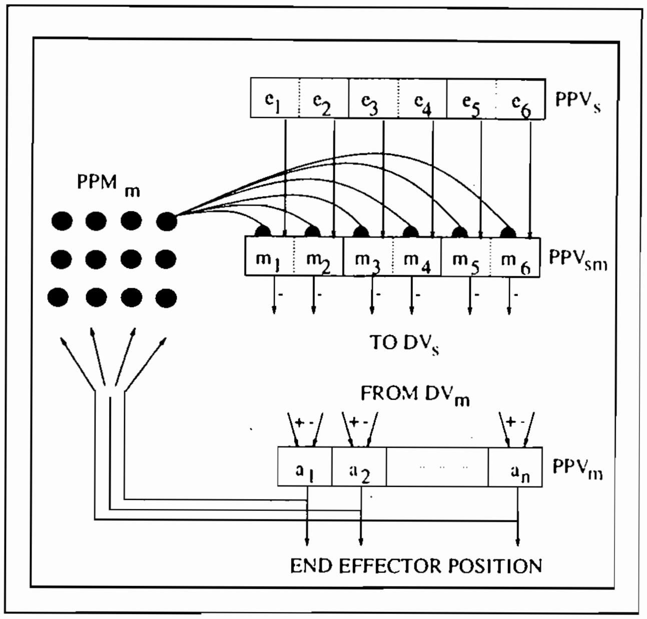

**Figure 12.** Scheme for learning a motor-to-spatial mapping that allows corollary discharge information from *PPV*$_m$ to specify end effector spatial position at *PPV*$_{sm}$ when visual feedback of end effector position is unavailable.

and the non-overlapping ranges $[d_j^{k-},d_j^{k+}]$ were smaller than the ranges used in Eq. (12). Each *PPM*$_m$ stage cell therefore responded maximally to a small neighborhood of limb configuration vectors *PPV*$_m$. All cells at the *PPM*$_m$ stage project, in turn, to the stage *PPV*$_{sm}$ via modifiable synapses.

These modifiable synapses learn the activities instated at the *PPV*$_{sm}$ stage by outputs of the *PPV*$_s$ stage. After learning, the internal feedback pathway *PPV*$_m$ → *PPM*$_m$ → *PPV*$_{sm}$ can substitute for the external visual pathway *PPV*$_m$ → End Effector Position → *PPV*$_s$ → *PPV*$_{sm}$. As shown in Section 3.6, this leads to the ability to perform blind reaches specified in spatial coordinates even if visual feedback is unavailable.

The six cell population activities $m_i$, $i = 1, \ldots, 6$, of the vector $M$ that represents end effector position at *PPV*$_{sm}$ are assumed to form three antagonistic pairs. At equilibrium, they obey the equation

$$m_i = \frac{\zeta e_i + \sum_k j_k Z_{ki}}{\zeta(e_i + e_l) + \sum_k j_k(Z_{ki} + Z_{kl})} \tag{18}$$

where $\zeta$ is a large gain constant for visual end effector data $E = (e_1, e_2, \ldots, e_6)$, $j_k$ is the activity of the $k$th cell in the *PPM*$_m$ stage, $Z_{ki}$ is the weight of the adaptive connection between $j_k$ and $m_i$, and the subscript $l$ denotes the index of the cell antagonistically paired with cell $i$. This equation ensures normalization of total activity distributed between each opponent pair. It is the type of normalization exhibited by feedforward on-center offsurround shunting networks (Grossberg, 1973, 1982). The use of a high gain pathway to ensure dominance of a visual input over another input to a normalized net was also used in Grossberg and Kuperstein (1986, 1989). In the present simulations, it is assumed that the gain constant $\zeta$ is large enough that the following approximations are valid. With visual feedback,

$$m_i = \frac{e_i}{e_i + e_I}, \quad 1 \leq i \leq 6 \tag{19}$$

In the absence of visual feedback,

$$m_i = \frac{\sum_k j_k Z_{ki}}{\sum_k j_k (Z_{ki} + Z_{kI})}, \quad 1 \leq i \leq 6 \tag{20}$$

The adaptive connections between the $PPM_{\mathrm{m}}$ stage and the $PPV_{\mathrm{sm}}$ stage were initialized at zero and modified according to the outstar learning law:

$$\frac{dZ_{ki}}{dt} = \eta j_k(-\kappa Z_{ki} + m_i) \tag{21}$$

where $\eta$ is a learning rate parameter, and $\kappa$ is a memory decay rate parameter. Parameter values $\eta = 1$ and $\kappa = 0.2$ were used in the simulations.

## 5. COMPARISONS WITH NEUROBIOLOGICAL DATA

Data from several recent neurophysiological studies of primate single cell properties in motor cortex and related areas are consistent with the approach to inverse kinematics used in the DIRECT model. A number of investigators have described cells in several motor areas, including the motor cortex (MC), supplementary motor area (SMA), and putamen, whose activity levels are dependent on movement direction (Georgopoulos et al., 1984; Kettner, Schwartz, & Georgopoulos, 1988; Kalaska, Cohen, Hyde, & Prud'homme, 1989; Alexander & Crutcher, 1990; Caminiti, Johnson, & Urbano, 1990). That these cells were indeed sensitive to movement direction rather than target positions was demonstrated by Kettner et al. (1988) who showed that changes in cell activity did not differ statistically for parallel movements from different origins. Evidence that some of these cells code *external* space direction rather than direction in joint or muscle space is found in Alexander and Crutcher (1990). In that study, monkeys were trained to move a mouse with their hand to cause a cursor to move to a target location on a monitor. On some trials the cursor moved in the same direction as the hand, while on other trials cursor movement was in the opposite direction than the hand movement. In addition to cells that fired preferentially for limb movements in a given direction, many cells were found which fired for a given direction of cursor movement *independent* of the limb movement direction that achieved this cursor movement. This result indicates that such cells are sensitive to movement direction in external space rather than joint space because they fire in concert with a movement direction in external space regardless of the movement direction in joint space. Cells whose activity was related to limb movement direction independent of cursor movement direction may have coded direction in either joint space or external space. Both possibilities are consistent with a system that maps spatial direction to joint angle increments.

Caminiti et al. (1990) studied movements in many directions within three distinct regions of the workspace, covering a much larger range of the workspace than that studied by Kettner et al. (1988). The regions were chosen such that a movement in a given spatial direction had to be carried out with different joint space movement directions in each of the three workspace regions. Motor cortical cells that were primarily related to shoulder movement were studied. Results showed that the preferred spatial direction of a given cell was different in different parts of the workspace. The changes in preferred directions when moving from one workspace region to another were orderly, with the rotation in preferred direction closely following the rotation of the shoulder joint between the two regions. The authors suggested that each of the studied cells commanded a synergy of muscle activity, and that the cell's preferred direction in different parts of the workspace corresponded to the direction of movement caused by instating this synergy. This is equivalent to defining preferred direction of the cell as a fixed direction in joint space.

Different interpretations of neurophysiological data lead to different alternatives for the direction-to-rotation mapping in the current model. Figure 13 illustrates three possible schemes for learning this mapping, with fixed weight connections indicated by arrows and adaptive weight connections indicated by semicircles. Figure 13a illustrates the mapping scheme used in the above simulations. In this scheme, cells sensitive to a particular motion direction and joint configuration ($PDM_{\mathrm{ms}}$ cells in Fig. 4) each learns a "synergy" of joint angle increments that is effective in producing this motion direction when the arm is in the appropriate joint configuration. In Figure 13b, learning occurs between $PDM_{\mathrm{ms}}$ cells and prewired "microsynergies" spanning several joints. Movement is specified by change in a $PPV_{\mathrm{m}}$ command resulting from integration of all active microsynergy inputs. In this scheme, a "synergy" for a given movement can be thought of as the summed effect of all microsynergies active during that movement. Simulations using this scheme have also proven successful in controlling planar movements by a three joint arm. Figure 13c shows a third possibility based on a model developed by Burnod et al. (1990) to explain data from the Caminiti et al. (1990) study described above. In this scheme, motor cortical cells with hard-wired, weighted connections to many muscles, akin to the microsynergies in Figure 13b

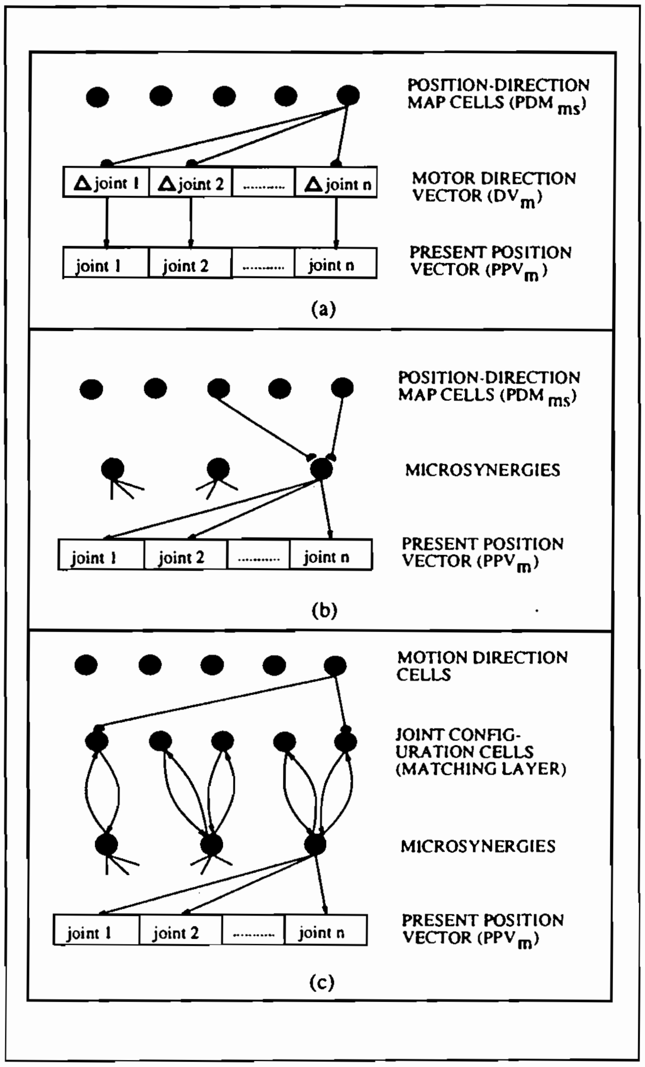
POSITION-DIRECTION MAP CELLS ($PDM_{ms}$)
Δjoint 1
Δjoint 2
..........
Δjoint n
MOTOR DIRECTION VECTOR ($DV_m$)
joint 1
joint 2
..........
joint n
PRESENT POSITION VECTOR ($PPV_m$)
(a)
POSITION-DIRECTION MAP CELLS ($PDM_{ms}$)
MICROSYNERGIES
joint 1
joint 2
..........
joint n
PRESENT POSITION VECTOR ($PPV_m$)
(b)
MOTION DIRECTION CELLS
JOINT CONFIG-URATION CELLS (MATCHING LAYER)
MICROSYNERGIES
joint 1
joint 2
..........
joint n
PRESENT POSITION VECTOR ($PPV_m$)
(c)

**Figure 13.** Three schemes for mapping between motion direction and muscle length or joint angle commands. Arrows indicate fixed-weight connections, and semicircles indicate adaptable connections.

are reciprocally connected with cells in a *matching layer*. The matching layer cells fire if the arm is in a particular configuration and either: (1) the "efference copy" input from an associated motor cortical cell is active due to spontaneous firing of that cell, or (2) input from cells specifying a desired motion direction is present. Learning of the mapping occurs by spontaneously activating a microsynergy, which indirectly activates a spatial direction cell by causing a movement, and directly activates a joint configuration cell through a reciprocal connection. The connections between the active spatial direction and joint configuration specific cells are then strengthened by learning. In all three circuits, joint angle or muscle velocity commands become associated with appropriate combinations of spatial direction and joint configuration.

Consideration of the Caminiti et al. (1990) data limits the cell types of Figure 13 that may be considered candidates for the observed motor cortical cells. These data showed cells that responded in many parts of joint space, thus eliminating cells whose activation is dependent upon a particular joint configuration. This leaves only the $DV_m$ cells from scheme (a) and the MICROSYNERGIES cells from schemes (b) and (c) as candidates for the motor cortex cells studied by Caminiti et al. (1990) and by Georgopoulos et al. (1984). This conclusion is in agreement with the interpretation of Bullock and Grossberg (1988a; see also 1991) and Mussa-Ivaldi (1988).

The primary difference between scheme (a) and schemes (b) and (c) concerns the action of the hypothesized motor cortical cells on spinal motoneurons. Specifically, do individual motor cortical cells influence a motoneuron pool innervating several muscles as in schemes (b) and (c), or only a particular muscle as in scheme (a)? The biological data concerning this issue are inconclusive. Early experiments that relied on stimulation of the cortical surface seemed to indicate that local areas in motor cortex induce activity in several muscles. By stimulating deep pyramidal cells directly, however, Asanuma and Sakata (1967) showed that very low stimulation currents resulted in activation of a single muscle, whereas significantly higher currents, up to five times as large as those required for single muscle activity, were required to cause activity in more than one muscle. Some recent investigators have nonetheless reported that motor cortical cells might influence muscle combinations. For example, Schwartz, Kettner, and Georgopoulos (1988) stated that their evidence "suggests that motor cortical cells might relate to *weighted combinations of muscles*. . . . This arrangement would provide a rich substrate for the motor cortical control of multidimensional arm movements" (p. 2926). In any case, the success of simulations using both schemes (a) and (b) indicates that many anatomies along the continuum from strictly single muscle activation to multijoint activation cells can successfully self-organize and will possess the robustness exhibited in these simulations.

The current model provides insight into another aspect of these neurophysiological data. Many neurophysiologists have reported that motor cortical cells seem to be broadly tuned to desired direction of movement. Thus, a motor cortical cell fires with maximal response rate for movement in a particular preferred direction, and at progressively lower rates for movement directions farther away from the preferred direction. Schwartz et al. (1988) fit their data with a *directional tuning function* in which response rate is a linear function of the cosine of the angle between the cell's preferred direction and the actual direction of the movement. Two possible interpretations of this phenomenon arise within the context of the current model. In the first interpretation, information specifying the desired movement direction may be broadly tuned. Then, instead of only becoming active for a small range of desired movement directions, individual $PDM_{ms}$ cells would be tuned to respond with the broad tuning curve reported by Schwartz et al.

(1988). Computer simulations using this approach have, however, invariably resulted in movement trajectories that deviated greatly from the desired movement trajectory. Though such results suggest the need for relatively sharply tuned directional information for accurate performance of a desired trajectory, we are exploring the feasibility of relaxing this requirement.

A second interpretation of these data assumes that the broadly tuned motor cortical cells correspond to the $DV_m$ cells, as hypothesized above. Then, even if information specifying movement direction is sharply tuned at the $PDM_{ms}$ stage, measurement of response rates at the $DV_m$ cells will be broadly tuned to direction of movement. To see this, note that each $PDM_{ms}$ cell projects to all of the $DV_m$ cells in a weighted combination or synergy. Consider for simplicity only a small range of joint space. Within this range, each $DV_m$ cell is represented in many synergies corresponding to many motion directions. Activation of a particular $DV_m$ cell will cause a particular motion direction of the end effector, corresponding to the $DV_m$ cell's preferred direction. The projection to this $DV_m$ cell from the corresponding $PDM_{ms}$ cells will be large. The $PDM_{ms}$ cells that code nearby directions will have slightly smaller projections to this $DV_m$ cell and slightly larger projections to nearby $DV_m$ cells. As movement direction moves farther away from the preferred direction of the $DV_m$ cell, the cell's contribution to the synergy for the movement gradually grows smaller and smaller.

Figure 14 shows directional tuning curves of $DV_m$ cells after training in the above simulations. Figure 14a plots cell activity vs. the angular difference between movement direction and the cell's preferred direction for a typical $DV_m$ cell in one small area of joint space after training was complete. This curve was generated by sweeping through 360° of motion directions in thirty 12° increments near a single joint configuration, then calculating the resulting $DV_m$ cell activation for each direction. Despite the fact that very sharp directional tuning was used to specify motion direction, the directional tuning curves of the $DV_m$ cells show the broad tuning characteristic of motor cortical cells. Indeed, the solid line in Figure 14b indicates the average form of $DV_m$ tuning curves in the model after training. This curve was generated by averaging 500 curves as shown in Figure 14a. These 500 measurements were evenly distributed between the six $DV_m$ cells at different joint configurations, by sampling approximately 83 joint configurations per $DV_m$ cell. The broken line in Figure 14b shows an averaged tuning curve obtained from single cell measurements in primate motor cortex by Kalaska et al. (1989). This curve is very similar to the average curve measured for the model. Because the simulations were done in two dimensions with an arm whose geometry differs greatly from that of a monkey moving in three dimensions, a more quantitative analysis of these curves is not appropriate here.

The fact that sharp directional tuning at the $PDM_{ms}$ stage was successfully used to produce accurate trajectory performance leads to the following prediction: Broad directional tuning of motor cortical cells may be due to the distributed nature of the mapping from spatial directions to joint rotations, rather than to broad tuning of spatial direction at higher levels of the sensorimotor hierarchy. Further experimental analysis will be required to verify or refute this prediction.

## 6. COMPARISONS WITH OTHER APPROACHES TO REDUNDANT CONTROL

The process by which redundant DOFs are efficiently handled by the motor system was termed *sensorimotor coordination* by Bernstein (1967; see also Berkinblit, Feldman, and Fukson, 1986; Saltzman, 1979). The DIRECT model utilizes redundant DOFs in parallel to solve a task. If some of these DOFs are removed on a given trial by environmental or internal constraints, the system can automatically compensate without additional learning or recomputation by using the remaining DOFs to produce the movement. Sensorimotor coordination is attained by learning the effects of many possible actions utilizing all available DOFs of the system, then applying all or a subset of these actions in parallel to produce the desired effect. Thus the DIRECT approach treats redundancy as an advantage to be exploited on every reach.

A common alternative approach to controlling redundant systems is to treat the problem as one of reducing the redundant DOFs of the system by internally constraining the ways in which effectors can be used. This could involve "freezing" joints or specifying functional relationships between joints (Saltzman, 1979). For example, Soechting and Lacquaniti (1981, p. 719) offered the following interpretation of data showing that elbow angular velocity ($\dot{\phi}$) is linearly related to shoulder angular velocity ($\dot{\theta}$) in the latter stages of a reaching movement: "we note that, by introducing such a constraint ($\dot{\phi} = k\dot{\theta} + c$) the number of degrees of freedom of the system is reduced from two to one in the terminal phase of the movement, and thereby, the complexity of the problem may be reduced . . . . We suggest that the most economical solution to this control problem compatible with the data would entail the existence of a planned trajectory which would be subject to the constraint that elbow and shoulder velocity be related to each other linearly as the final position is approached." Such constraints are closely related to the classical concept of a *synergy*, or collection of joint motions controlled synchronously as a single unit.

The primary difficulty with the classical notion of a "synergy-based" approach is the lack of flexibility it affords when external constraints are imposed. If efficiently controlled, redundancy in a system provides the flexibility to handle the loss of some DOFs due to environmental constraints by using the remaining DOFs to solve

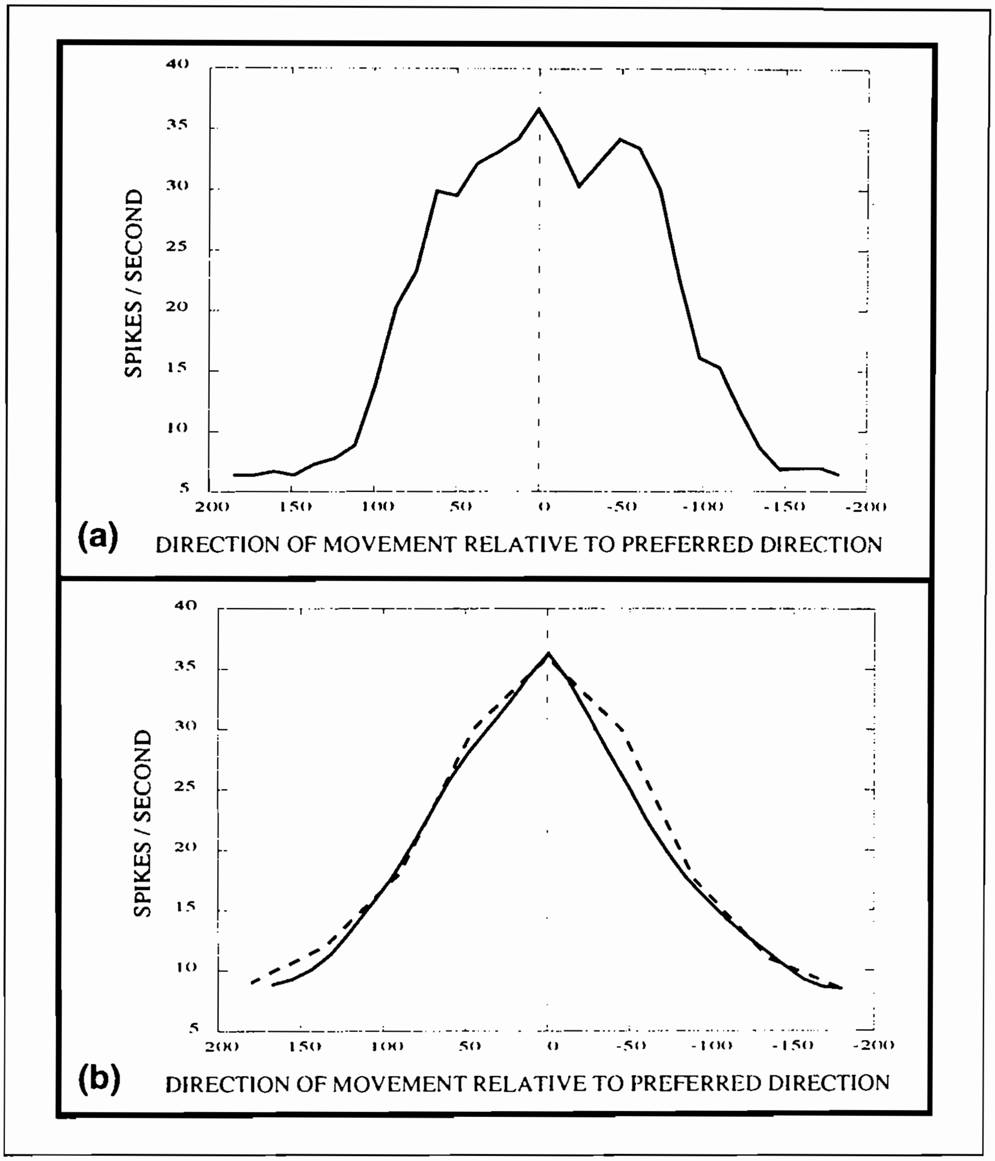

**Figure 14.** (**a**) Typical directional tuning curve for a DIRECT model $DV_m$ cell. (**b**) Directional tuning curve averaged over 500 measurements of the different joint velocity cells in different parts of joint space for the simulated model (solid line) and corresponding data from Kalaska et al. (1989) (broken line). Model data have been scaled to cover the same range as the Kalaska et al. data.

the task. Internal constraints, such as synergies that reduce the redundant system to a nonredundant system, destroy this flexibility.

Greene (1982) described a system that might circumvent this problem by breaking the control system into many control subsystems, each of which is proficient in controlling a nonredundant "virtual arm" formed from synergy-like constraints on movements of the actual arm. The problem of dealing with external constraints then becomes one of choosing a subsystem whose virtual arm allows completion of the task within these constraints. Although such a system is useful for many types of motions, it could prove cumbersome for reaches under unexpected external constraints since (1) it requires "mode switching" between subsystems when a chosen subsystem is rendered ineffective by an unexpected environmental constraint, and (2) its repertoire of virtual arms must be large enough to deal with a vast number of possible environmentally imposed constraints. Although neither of these criticisms forces rejection of Greene's proposal, it seems desirable for a system or subsystem to *automatically* deal with external constraints whenever possible without the need for mode-switching. Thus, although the existence of different modes of operation with different controllers is not denied here, the current approach attempts to provide compensation for unexpected events at a low level whenever possible, leaving higher processing levels free to perform other tasks.

Another common approach to controlling systems with redundant DOFs involves minimizing an objective function using well-known optimization algorithms such as steepest descent (as in backpropagation), Newton's method, or conjugate gradient methods to determine suitable parameter values for the controlling model; see Shanno (1990) for a review. In a redundant system, an objective function that deals only with the desired spatial goal is typically insufficient because there is no unique set of model parameters that minimize this function. Therefore, it is common practice to add additional constraints to the objective function to remove the redundancy and allow for a unique solution. These additional constraints are typically chosen to achieve desirable and/or commonly observed properties of the controlling system. For example, Jordan (1988) described a model incorporating a temporal smoothness constraint that helps to ensure that temporally adjacent actions do not conflict with each other. Kawato (1990) described a network that finds solutions to the inverse dynamics problem which satisfy a "minimum torque change" criterion. A model system governed by this criterion has been shown to accurately reproduce human reaching trajectories under certain conditions (Uno, Kawato, & Suzuki, 1989).

The current approach differs from these optimization approaches in that it seeks to maximize "on-line" compensation for new or unexpected constraints imposed by the environment. Consider for example the effect of freezing a joint just before a reaching movement begins. Although an optimization approach could be used to produce an acceptable trajectory that takes this new constraint into consideration, such an approach would involve relearning of system parameters. Like synergy-based approaches, optimization approaches that use additional constraints to do away with redundancy *before* considering externally imposed constraints lose the flexibility afforded by redundancy to handle these constraints when they arise later during performance. In the DIRECT model, by contrast, the solutions for unconstrained reaches are formed without sacrificing the flexibility afforded by redundancy. Furthermore, the choice of a direction-to-rotation mapping from 3-D space to joint space allows the system to effectively use this redundancy to deal with unexpected events in the environment, without *any* relearning of model parameters. Such on-line compensation without destruction of previous learning is essential for biological systems, which must deal with a variety of unexpected environmental conditions quickly and flexibly.

Models of Hinton (1984) and Berkinblit, Gelfand, and Feldman (1986) considered some concepts similar to those in the current model. In Hinton (1984), however, the difficult inverse kinematics problem for redundant manipulators is not addressed because the joint angle changes that move the arm are formulated simply by calculating the torques and resulting angle changes that would occur at each angle if the arm was "pulled" directly toward the target. Nonetheless, this model contains two interesting properties that are relevant to the current model. First, Hinton demonstrated that two tasks (e.g., maintaining balance and reaching toward the target) could be simultaneously performed by independently inducing joint angle increments that work to complete them, even if the tasks each require increments to the same joints. This is done by weighted addition of the increments that are specified by the different tasks to a given joint. This result is pertinent to the DIRECT model because it outlines a method for incorporating other motor constraints, such as maintaining balance during a reach, simultaneously with reaching movements. Hinton (1984) also noted that the number of iterations to task completion could be reduced if combinations of joint increments whose side-effects cancel out, such as movements in directions orthogonal to the desired movement direction, are used in addition to increments to individual joints. This concept of synergies differs from the more common treatment, in which synergies reduce the number of DOFs that need to be controlled. The synergies in Hinton's model increase efficiency rather than decrease the number of DOFs. The DIRECT model takes this concept a step further by initiating *only* appropriate synergies, essentially eliminating unwanted side effects under normal conditions. The model accomplishes this by solving a fundamental problem not dealt with by Hinton; namely, how does the system know which synergies to apply in a given situation, given that the usefulness of a given synergy is dependent on current joint configuration and movement direction? The DIRECT model learns which movement directions a synergy produces in different parts of the workspace under on-line movement conditioning and later uses the synergies derived from this learning. By experiencing a large enough number of synergies, the system becomes capable of choosing appropriate sets of synergies to produce desired movement directions throughout the workspace.

Berkinblit et al. (1986b) described a model that controls planar movements of a 3-joint limb. This model solves the inverse kinematics problem for a redundant manipulator by independently calculating joint angle increments according to the following equation:

$$\dot{\theta}_i = k_i[\mathbf{D}, \mathbf{W_i}] = k_i\|\mathbf{D}\|\|\mathbf{W_i}\|\sin \alpha_i \qquad (22)$$

$i = 1,2,3$, where $\theta_i$ is the angle of the $i$th joint, $[\mathbf{D}, \mathbf{W_i}]$ is the cross product of the desired movement vector $\mathbf{D}$ and the joint's *working vector* $\mathbf{W_i}$, $k_i$ is a constant, and $\alpha_i$ is the angle between $\mathbf{D}$ and $\mathbf{W_i}$. The working vector of a joint is defined as the spatial vector between the center of rotation of the joint and the endpoint of the arm. This model displays robustness to "freezing" of a joint as well as motor equivalence in the sense that it can reach a target with many different final joint configurations. One significant drawback of this model, however, is that the trajectory produced by Eq. (22) does not accurately move the end effector along the desired movement vector toward the target. This is because the model computes each $\theta_i$ independently; there is no mechanism for controlling the *combined* effects of the $\theta_i$ rotations to move the arm in the desired direction. As a result, the system does not have an accurate mapping between end effector movement directions and the joint angle changes that produce those movement directions. Instead, angle increments are chosen that move the end effector in the general direction of the target. The end effector will consequently approach the target, but its trajectory cannot be controlled accurately. Most skilled motor tasks, such as handwriting or tracing, do require accurate control over the direction of end effector motion, as provided by DIRECT.

The models of Hinton (1984) and Berkinblit, Gelfand, and Feldman (1986) also do not address some important issues concerning control of movement in biological systems. Unlike these models, the DIRECT model suggests how a neural controller can develop without a priori knowledge of the relationship between joint movements and the 3-D spatial results of such movements, how sensory data indicative of end effector position can be combined from different modalities, how this sensory information can drive and shape ongoing movement, and how the system can continually retune its transformations to deal with changes in effector properties. Moreover, all the inputs to the DIRECT model are readily available in the sensorimotor environment. By contrast, it is not clear how an organism would gain access to information about the spatial coordinate working vector for each of its joints.

Mel (1990; pp. 17, 66–68) briefly described a scheme for learning a redundant mapping from motion directions to joint angle perturbations of a robotic arm that is similar to the mapping scheme in the current work. As this mapping was not the focus of Mel (1990), few implementational details were given, and the motor equivalent properties of this mapping were not explored. The present work has investigated the properties of such a mapping as they relate to motor equivalent human performance, describes in detail how such a mapping can naturally arise in biological systems, and compares model cells to cell data from neurophysiological experiments.

## CONCLUDING REMARKS

The current approach may prove useful in the study of motor equivalence and sensorimotor coordination in other modalities. For example, eye–head coordination has a natural interpretation within the framework of the current model. Target specification in body-centered coordinates results in a spatial DV, and this spatial DV maps to both neck muscles and eye muscles whose activation can zero the DV. If, for example, the neck muscles are made ineffective by immobilizing the head using a bitebar, the eye muscles could still complete the movement even though attempts to move the head are unsuccessful. The current approach has also been extended to speech production (Guenther, 1992).

Further development of the DIRECT model will investigate how the model can retain the kinematic properties characteristic of human and monkey movement trajectories that have elsewhere been explained using the VITE model (Bullock & Grossberg, 1988a, 1988b, 1989, 1991). In the current, simplified implementation, activity at the $PDM_{ms}$ stage is all or none, so additional structure is required to ensure that the magnitude of the $DV_m$ is proportional to the magnitude of the $DV_s$, as in the VITE model. One aspect of this synthesis has been explored in the VITEWRITE model of Bullock, Grossberg, and Mannes (1992), which shows how a motor program that generates appropriately timed directional commands such as those computed by DIRECT can produce fluent handwriting that exhibits many properties of human psychophysical data.

The present model instantiation indicates the types and ordering of vector stages and map stages that are competent to generate the motor equivalence properties characteristic of flexible planned movements. Perhaps most significantly, by explaining positionally accurate tool use as a consequence of a general competence for motor equivalent action, the model begins to clarify how this important property of primate and human social groups may have emerged during the evolutionary process.

## APPENDIX A: KINEMATIC EQUATIONS

Figure 15 defines the different coordinate frames used in the simulated model. For forward kinematics, joint angle coordinates ($\theta_1$, $\theta_2$, $\theta_3$) are first transformed into Cartesian coordinates ($X$, $Y$), then into the spherical coordinates ($R$, $\phi$) corresponding to the internal representation of 3-D space described in Section 4.1. The following equations define the transformation from joint angles to Cartesian coordinates for the end effector:

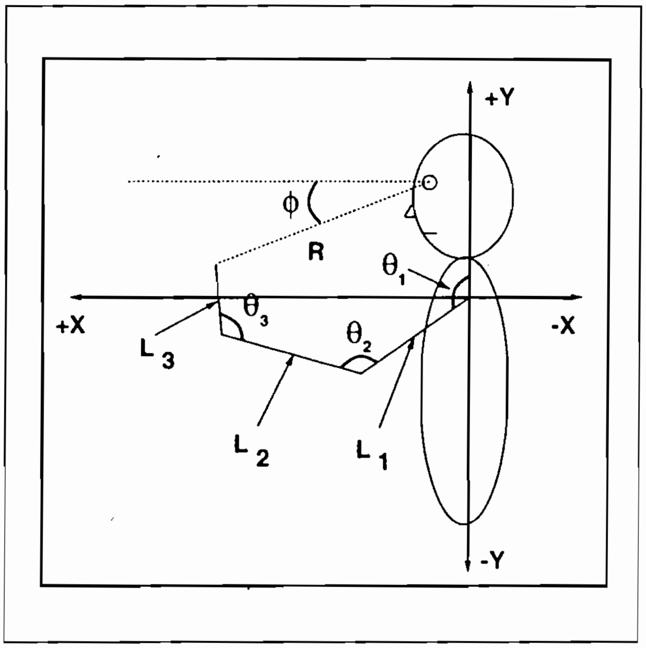

**Figure 15.** Coordinate definitions for the simulated model.

$$x_{ee} = L_1 \sin \theta_1 + L_2 \sin (\theta_1 + \theta_2 - \pi) + L_3 \sin (\theta_1 + \theta_2 + \theta_3) \quad (23)$$

$$y_{ee} = L_1 \cos \theta_1 + L_2 \cos (\theta_1 + \theta_2 - \pi) + L_3 \cos (\theta_1 + \theta_2 + \theta_3) \quad (24)$$

where $L_i$ is the length of arm segment $i$. For the simulations, realistic lengths and angle ranges were chosen for the arm: $L_1 = L_2 = 280$ mm, $L_3 = 160$ mm, $30° < \theta_1 < 240°$, $30° < \theta_2 < 180°$, and $30° < \theta_3 < 190°$.

If a tool is added to the hand, end effector Cartesian position becomes

$$x_{ee} = L_1 \sin \theta_1 + L_2 \sin (\theta_1 + \theta_2 - \pi) + L_3 \sin (\theta_1 + \theta_2 + \theta_3) + L_{\text{tool}} \sin (\theta_1 + \theta_2 + \theta_3 + \theta_{\text{tool}} - \pi) \quad (25)$$

$$y_{ee} = L_1 \cos \theta_1 + L_2 \cos (\theta_1 + \theta_2 - \pi) + L_3 \cos (\theta_1 + \theta_2 + \theta_3) + L_{\text{tool}} \cos (\theta_1 + \theta_2 + \theta_3 + \theta_{\text{tool}} - \pi) \quad (26)$$

where $L_{\text{tool}}$ and $\theta_{\text{tool}}$ are the length and angle of the tool, respectively.

The transformation from Cartesian to spherical coordinates is defined by the following equations:

$$R = \sqrt{(x_{ee} - x_{eye})^2 + (y_{ee} - y_{eye})^2} \quad (27)$$

$$\phi = \arctan \left( \frac{y_{eye} - y_{ee}}{x_{ee} - x_{eye}} \right) \quad (28)$$

## Acknowledgments

Daniel Bullock and Stephen Grossberg were supported in part by the National Science Foundation (NSF IRI 90-24877) and the Office of Naval Research (ONR N00014-92-J-1309). Frank Guenther was supported in part by the Air Force Office of Scientific Research (AFOSR F49620-92-J-0499) and the National Science Foundation (NSF IRI 90-24877). The authors wish to thank Kelly Dumont, Carol Jefferson, and Robin Locke for their valuable assistance in the preparation of the manuscript.

Reprint requests should be sent to Professor Stephen Grossberg, Department of Cognitive and Neural Systems, Boston University, 111 Cummington St., Boston, Massachusetts 02215.

## REFERENCES

Abbs, J. H., & Gracco, V. L. (1984). Control of complex motor gestures: Orofacial muscle responses to load perturbations of lip during speech. *Journal of Neurophysiology, 51*(4), 705–723.

Alexander, G. E., & Crutcher, M. D. (1990). Neural representations of the target (goal) of visually guided arm movements in three motor areas of the monkey. *Journal of Neurophysiology, 64*(1), 164–178.

Anderson, R. A., Essick, G. K., & Siegel, R. M. (1985). Encoding of spatial location by posterior parietal neurons. *Science, 230,* 456–458.

Asanuma, H., & Sakata, H. (1967). Functional organization of a cortical efferent system examined with focal depth stimulation in cats. *Journal of Neurophysiology, 30,* 35–54.

Berkinblit, M. B., Feldman, A. G., & Fukson, O. I. (1986). Adaptability of innate motor patterns and motor control mechanisms. *Behavioral and Brain Sciences, 9,* 585–638.

Berkinblit, M. B., Gelfand, I. M., & Feldman, A. G. (1986). Model of the control of the movements of a multijoint limb. *Biophysics, 31*(1), 142–153.

Bernstein, N. A. (1967). *The co-ordination and regulation of movements.* New York: Pergamon.

Bock, O., & Eckmiller, R. (1986). Goal-directed arm movements in absence in visual guidance: Evidence for amplitude rather than position control. *Experimental Brain Research, 62,* 451–458.

Bullock, D., & Contreras-Vidal, J. (1992). How spinal neural networks reduce discrepancies between motor intention and motor realization. In K. M. Newell & D. M. Corcos (Eds.), *Variability and motor control.* Champaign, IL: Human Kinetics Press.

Bullock, D., Contreras-Vidal, J., & Grossberg, S. (1992). Equilibria and dynamics of a neural network model for opponent muscle control. In G. Bekey & K. Goldberg (Eds.), *Neural networks in robotics.* Boston: Kluwer Academic.

Bullock, D., Greve, D., Grossberg, S., & Guenther, F. H. (1992). A head-centered representation of 3-D target location derived from opponent eye position commands. In *Proceedings of the International Joint Conference on Neural Networks,* Baltimore, MD, 1992 (Vol. I, pp. 79–85). Piscataway, NJ: Institute of Electrical and Electronics Engineers.

Bullock, D., & Grossberg, S. (1988a). Neural dynamics of planned arm movements: Emergent invariants and speed-accuracy properties during trajectory formation. *Psychological Review, 95*(1), 49–90.

Bullock, D., & Grossberg, S. (1988b). The VITE model: A neural command circuit for generating arm and articulator trajectories. In J. A. S. Kelso, A. J. Mandell, & M. F. Shlesinger (Eds.), *Dynamic patterns in complex systems.* Singapore: World Scientific Publishers.

Bullock, D., & Grossberg, S. (1989). VITE and FLETE: Neural modules for trajectory formation and postural control. In W. A. Hershberger (Ed.), *Volitional action.* Amsterdam: North-Holland-Elsevier.

Bullock, D., & Grossberg, S. (1991). Adaptive neural networks for control of movement trajectories invariant under speed and force rescaling. *Human Movement Science, 10,* 3–53.

Bullock, D., Grossberg, S., & Guenther, F. H. (1992). A self-organizing neural network model for redundant sensory-motor control, motor equivalence, and tool use. In *Proceedings of International Joint Conference on Neural Networks,* Baltimore, MD, 1992 (Vol. IV, pp. 91–96). Piscataway, NJ: Institute of Electrical and Electronics Engineers.

Bullock, D., Grossberg, S., & Mannes, C. (1992). *A neural network model for cursive script production.* Technical Report CAS/CNS-TR-92-029. Boston, MA: Boston University. *Biological Cybernetics,* in press.

Burnod, Y., Caminiti, R., Johnson, P., Granguillaume, P., & Otto, I. (1990). Model of visuo-motor transformations performed by the cerebral cortex to command arm movements at visual targets in the 3-D space. In R. Eckmiller (Ed.), *Advanced neural computers* (pp. 33–41). Amsterdam: Elsevier Science Publishers.

Caminiti, R., Johnson, P., & Urbano, A. (1990). Making arm movements within different parts of space: Dynamic aspects in the primate motor cortex. *The Journal of Neuroscience, 10,* 2039–2058.

Clark, D. M., & Ravishankar, K. (1990a). A convergence theorem for Grossberg learning. *Neural Networks, 3,* 87–92.

Clark, D. M., & Ravishankar, K. (1990b). Acquisition and decay rates in synaptically coded memory. *Neural Networks, 3,* 525–534.

Desimone, R., & Ungerleider, L. G. (1989). Neural mechanisms of visual processing in monkeys. In F. Boller & J. Grafman (Eds.), *Handbook of neuropsychology* (Vol. 2, Chapter 14, pp. 267–299. Amsterdam: Elsevier.

Evarts, E. V., & Tanji, J. (1974). Gating of motor cortex reflexes by prior instruction. *Brain Research, 71,* 479–494.

Flash, T. (1989). Generation of reaching movements: Plausibility and implications of the equilibrium trajectory hypothesis. *Brain, Behavior and Evolution, 33,* 63–68.

Flash, T., & Hogan, N. (1985). The coordination of arm movements: An experimentally confirmed mathematical model. *The Journal of Neuroscience, 5,* 1688–1703.

Fu, Q.-G., Suarez, J. I., & Ebner, T. J. (1992). Neuronal specification of direction and distance during reaching movements in the superior precentral premotor area and primary motor cortex in monkeys. Submitted for publication.

Gaudiano, P., & Grossberg, S. (1991). Vector associative maps: Unsupervised real-time error-based learning and control of movement trajectories. *Neural Networks, 4*(2), 147–183.

Georgopoulos, A. P., (1986). On reaching. *Annual Review of Neuroscience, 9,* 147–170.

Georgopoulos, A. P. (1989). Motor cortex and reaching. In M. Ito (Ed.), *Neural programming*, (pp. 3–12). Basel: Karger.

Georgopoulos, A. P., Kalaska, J. F., Caminiti, R., & Massey, J. T. (1982). On the relations between the direction of two-dimensional arm movements and cell discharge in primate motor cortex. *Journal of Neuroscience, 2*(11), 1527–1537.

Georgopolous, A. P., Kalaska, J. F., Crutcher, M. D., Caminiti, R., & Massey, J. T. (1984). The representation of movement direction in the motor cortex: Single cell and population studies. In G. M. Edelman, W. E. Gall, & W. M. Cowan (Eds.), *Dynamic aspects of cortical function* (pp. 501–524). New York: Wiley.

Georgopolous, A. P., Schwartz, A. B., & Kettner, R. E. (1986). Neuronal population coding of movement direction. *Science, 233,* 1416–1419.

Goodale, M. A., & Milner, D. (1992). Separate visual pathways for perception and action. *Trends in Neurosciences, 15,* 20–25.

Greene, P. H. (1982). Why is it easy to control your arms? *Journal of Motor Behavior, 14*(4), 260–286.

Greve, D., Grossberg, S., Guenther, F. H., & Bullock, D. (1992). Neural representations for sensory-motor control I: Head-centered 3-D target positions for opponent eye commands. *Acta Psychologica 82,* 115–138.

Grossberg, S. (1968). Some nonlinear networks capable of learning a spatial pattern of arbitrary complexity. *Proceedings of the National Academy of Sciences USA, 59*(2), 368–372.

Grossberg, S. (1969). On learning and energy-entropy dependence in recurrent and noncurrent signed networks. *Journal of Statistical Physics, 1,* 319–350.

Grossberg, S. (1973). Contour enhancement, short-term memory, and constancies in reverberating neural networks. *Studies in Applied Mathematics, 52,* 217–257.

Grossberg, S. (1976). Adaptive pattern classification and universal recoding, I: Parallel development and coding of neural feature detectors. *Biological Cybernetics, 23,* 121–134.

Grossberg, S. (1982). *Studies of mind and brain: Neural principles of learning, perception, development, cognition, and motor control.* Boston: Reidel.

Grossberg, S. (1986). The adaptive self-organization of serial order in behavior: Speech, language, and motor control. In E. C. Schwab & H. C. Nusbaum (Eds.), *Pattern Recognition by humans and machines, I: Speech perception* (pp. 187–294). New York: Academic Press. Reprinted in Grossberg, S. (1987). *The adaptive brain, II: Vision, speech, language, and motor control.* Amsterdam: North-Holland.

Grossberg, S. (1989). Neural network models of vector coding, learning, and trajectory formation during planned and reactive arm and eye movements. In M. Ito (Ed.), *Neural programming* (pp. 223–247). Tokyo: Japan Scientific Societies Press. New York: Karger. Also see Grossberg, S., & Kuperstein, M. (1989). *Neural dynamics of adaptive sensory-motor control, expanded edition* (Chapter 14). Elmsford, NY: Pergamon Press.

Grossberg S., Guenther, F. H., Bullock, D., & Greve, D. (1992). Neural representations for sensory-motor control II: Learning a head-centered visuomotor representation of 3-D target positions. *Neural Networks 6,* 43–68.

Grossberg, S., & Kuperstein, M. (1986). *Neural dynamics of adaptive sensory-motor control: Ballistic eye movements.* Amsterdam: North-Holland.

Grossberg, S., & Kuperstein M. (1989). *Neural dynamics of sensory-motor control, expanded edition.* Elmsford, NY: Pergamon Press.

Guenther, F. H. (1992). *Neural models of adaptive sensory-motor control for flexible reaching and speaking.* Unpublished Doctoral thesis. Boston, MA: Boston University.

Guenther, F. H., Bullock, D., Greve, D., & Grossberg, S. (1992). Neural representations for sensory-motor control III: Learning a body-centered visuomotor representation of 3-D target positions. Submitted for publication.

Hinton, G. (1984). Parallel computations for controlling an arm. *Journal of Motor Behavior, 16*(2), 171–194.

Hollerbach, J. M., Moore, S. P., & Atkeson, C. G. (1986). Workspace effect in arm movement kinematics derived by joint interpolation. In G. Gantchev, B. Dimitrov, & P. Patev (Eds.), *Motor control* (pp. 197–208). New York: Plenum.

Howarth, C. I., & Beggs, W. D. A. (1972). The relationship between speed and accuracy of movement aimed at a target. *Acta Psychologia, 35,* 207–218.

Hubel, D. H., & Wiesel, T. N. (1977). Functional architecture of macaque monkey visual cortex. *Proceedings of the Royal Society of London (B), 198,* 1–59.

Jordan, M. I. (1988). *Supervised learning and systems with excess degrees of freedom.* (COINS Tech. Rep. 88-27). Amherst, MA: University of Massachusetts, Computer and Information Sciences.

Kalaska, J. F., Cohen, D. A. D., Hyde, M. L., & Prud'homme, M. (1989). A comparison of movement direction-related versus load direction-related activity in primate motor cortex, using a two-dimensional reaching task. *Journal of Neuroscience, 9*(6), 2080–2102.

Kawato, M. (1990). Computational schemes and neural network models for formation and control of multijoint arm trajectory. In W. T. Miller, III, R. S. Sutton, & P. J. Werbos (Eds.), *Neural networks for control* (pp. 197–228). Cambridge, MA: MIT Press.

Kelso, J. A. S., Tuller B., Vatikiotis-Bateson, E., & Fowler, C. A. (1984). Functionally specific articulatory cooperation following jaw perturbations during speech: Evidence for coordinative structures. *Journal of Experimental Psychology: Human Perception and Performance, 10*(6), 812–832.

Kettner, R. E., Schwartz, A. B., & Georgopolous, A. P. (1988). Primate motor cortex and free arm movements to visual targets in three-dimensional space. III. Positional gradients and population coding of movement direction from various movement origins. *Journal of Neuroscience, 8*(8), 2938–2947.

Kohonen, T. (1988). *Self-organization and associative memory*, 2nd Ed. New York: Springer-Verlag.

Lacquaniti, F., Ferrigno, G., Pedotti, A., Soechting, J. F., & Terzuolo, C. (1987). Changes in spatial scale in drawing and handwriting: Kinematic contributions by proximal and distal joints. *Journal of Neuroscience, 7*(3), 819–828.

Lacquaniti, F., Soechting, J. F., & Terzuolo, C. A. (1982). Some factors pertinent to the organization and control of arm movements. *Brain Research, 252*, 394–397.

Malsburg, C. von der (1973). Self-organization of orientation sensitive cells in the striate cortex. *Kybernetik, 14*, 85–100.

Mays, L., & Sparks, D. (1980). Saccades are spatially, not retinocentrically, coded. *Science, 208*, 1163–1165.

Mays, L., & Sparks, D. (1981). The localization of saccade targets using a combination of retinal and eye position information. In A. F. Fuchs & W. Becker (Eds.), *Progress in oculomotor research* (pp. 39–47). New York: Elsevier/North-Holland.

Mel, Bartlett W. (1990). *Connectionist robot planning: A neurally-inspired approach to visually-guided reaching*. Boston: Academic Press.

Morasso, P. (1981). Spatial control of arm movements. *Experimental Brain Research, 42*, 223–227.

Morasso, P. (1986). Trajectory formation. In P. Morasso & V. Tagliasco (Eds.), *Human movement understanding*. Amsterdam: North Holland.

Mountcastle, V. B. (1957). Modality and topographic properties of single neurons of cats somatic sensory cortex. *Journal of Neurophysiology, 20*, 408–434.

Mussa-Ivaldi, F. A. (1988). Do neurons in the motor cortex encode movement direction? An alternative hypothesis. *Neuroscience Letters, 91*, 106–111.

Nagasaki, H. (1989). Asymmetric velocity and acceleration profiles of human arm movements. *Experimental Brain Research, 74*, 319–326.

Ott, D., & Eckmiller, R. (1988). Dynamic adaptation of the blind pointing characteristic to stepwise lateral tilts of body, head, and trunk. *Behavioral Brain Research, 30*, 99–110.

Piaget, J. (1963). *The origins of intelligence in children*. New York: Norton.

Saltzman, E. (1979). Levels of sensorimotor representation. *Journal of Mathematical Psychology, 20*, 91–163.

Schwartz, A. B., Kettner, R. E., & Georgopoulos, A. P. (1988). Primate motor cortex and free arm movements to visual targets in three-dimensional space. I. Relations between single cell discharge and direction of movement. *Journal of Neuroscience, 8*(8), 2913–2927.

Shanno, D. F. (1990). Recent advances in numerical techniques for large scale optimization. In W. T. Miller III, R. S. Sutton, & P. J. Werbos (Eds.), *Neural networks for control* (pp. 171–178). Cambridge, MA: MIT Press.

Soechting, J. F., & Flanders, M. (1989). Errors in pointing are due to approximations in sensorimotor transformations. *Journal of Neurophysiology, 62*(2), 595–608.

Soechting, J. F., & Lacquaniti, F. (1981). Invariant characteristics of a pointing movement in man. *Journal of Neuroscience, 1*(7), 710–720.

Sparks, D. L. (1978). Functional properties of neurons in the monkey superior colliculus: Coupling of neuronal activity and saccade onset. *Brain Research, 156*, 1–16.

Sparks, D. L. (1991). The neural encoding of the location of targets for saccadic eye movements. In J. Paillard (Ed.), *Brain and space* (pp. 3–19). New York: Oxford.

Sparks, D. L., & Jay, M. (1987). The role of the primate superior colliculus in sensorimotor integration. In M. A. Arbib & A. R. Hanson (Eds.), *Vision, brain, and cooperative computation* (pp. 109–128). Cambridge, MA: MIT Press.

Sparks, D. L., & Mays, L. E. (1981). The role of the monkey superior colliculus in the control of saccadic eye movements: A current perspective. In A. F. Fuchs & W. Becker (Eds.), *Progress in oculomotor research*. Amsterdam: Elsevier North-Holland.

Tanji, J., & Evarts, E. V. (1976). Anticipatory activity of motor cortex unit in relation to direction of an intended movement. *Journal of Neurophysiology, 39*, 1062–1068.

Teulings, H. L., Thomassen, A., & van Galen, G. P. (1986). Invariants in handwriting: The information contained in a motor program. In Kao, van Galen, & Hoosian (Eds.), *Graphonomics: Contemporary research in handwriting* (pp. 305–315). Amsterdam: Elsevier.

Ungerleider, L. G., & Mishkin, M. (1982). Two cortical visual systems: Separation of appearance and location of objects. In D. L. Ingle, M. A. Goodale, & R. J. W. Mansfield (Eds.), *Analysis of visual behavior* (pp. 549–586). Cambridge, MA: MIT Press.

Uno, Y., Kawato, M., & Suzuki, R. (1989). Formation and control of optimal trajectory in human multijoint arm movement: Minimum torque-change model. *Biological Cybernetics, 61*, 89–101.

Willshaw, D. J., & Malsburg, C. von der (1976). How patterned neural connections can be set up by self organization. *Proceedings of the Royal Society of London (B), 194*, 431–445.

Wise, S. P., & Desimone, R. (1988). Behavioral neurophysiology: Insights into seeing and grasping. *Science, 242*, 736–741.

Woodworth, R. S. (1899). The accuracy of voluntary movement. *Psychological Review, 3*, 1–114.